The influence of amplitude and phase variations on a resonant cavity

van Lierop, C.M.M.

Award date:
2003

TU/e technische universiteit eindhoven

Eindhoven University of Technology

Department of Electrical Engineering
Control Systems
P.O. Box 513
5600 MB Eindhoven

The influence of amplitude and phase variations on a resonant cavity.

Ing. C.M.M. van Lierop

January 2003

Internship report of the period March 2002 - January 2003.

Group : Control Systems
Supervisors : Ing. F.B. Kiewiet
A.H. Kemper
Dr. ir. O.J. Luiten
Prof. dr. M.J. van der Wiel
Prof. dr. ir. P.P.J. van den Bosch

Abstract

At Eindhoven University of Technology a project has been started to build a combined DC/RF accelerator. The RF accelerator cavity is an RF coupled resonant structure which creates a longitudinal electric field of standing waves (along the axis of the cavity). A pulsed laser is used to create a short bunch of electrons (photo emission). For optimal acceleration the electrons have to start at the right phase of the RF field. In order to achieve this the laser pulses have to be synchronized to the RF signal. The RF cavity is filled with energy by a pulsed klystron tube (which is an RF amplifier just like for instance a magnetron). To create an RF power pulse the power input of the klystron tube is pulse modulated. The modulator creates a pulse of approximately $20MW$ with a duration of $4\mu s$. The RF power pulse at the output of the klystron has a peak power of approximately $10MW$.

Usually the modulator is designed to deliver a flat top power pulse. In the setup which is built at Eindhoven University of Technology a different approach is used. Instead of using a modulator creating a flat top pulse the modulator was designed to create an "exponentially shaped" pulse. The reasons for choosing an "exponentially shaped" pulse instead of a flat top pulse are:

- only one short electron bunch is accelerated per RF power pulse (which consumes only a very small fraction of the power) so there is no need for a constant output power.
- the modulator becomes very compact because it contains less large high voltage and high power components.
- the modulator becomes more reliable mainly because it contains less capacitors.
- the modulator becomes cheaper.

However there are problems connected with using an "exponentially shaped" pulse to power the klystron tube. Firstly, the tube introduces a frequency change. This is caused by the changing acceleration voltages in the klystron which causes the output frequency of the klystron tube to shift with respect to its input frequency. Since the RF accelerator cavity has an extremely small bandwidth the changing delay causes the cavity to be shifted off resonance which means that the maximum RF field in the cavity will be smaller.

The second problem is that because of the changing frequency the phase of the RF field inside of the cavity will have a small time-dependency which could increase the phase jitter between the laser and the RF field inside the cavity. This might spoil the stability of the accelerator.

The third problem is caused by the shape of the pulse itself. Since the cavity has a very high quality factor it has a limited bandwidth which prevents it from reaching its maximum (steady state) value. This also results in a decrease of the maximum RF field inside the cavity.

These effects where analyzed in this report. The overall decrease of the electric RF field inside the cavity when using an "exponentially shaped" modulator pulse, equals approximately 10% of which approximately 5% is caused by the klystron output frequency change. The 5% loss of electric field due to phase changes is actually much less than the initial guess. There is one main reasons why the phase influence is much less than initially expected. The phase changes are caused by changes of the beam velocity inside the klystron. The relativistic effect reduces the phase variations around maximum because it can be seen as a saturation effect.

The phase jitter is slightly larger when using an "exponentially shaped" modulator pulse instead of a flat modulator pulse. The total time jitter resulting from the phase jitter has a standard deviation of approximately $3.9 \cdot 10^2 fs$. When using a flat top pulse the standard deviation of the total jitter could have been approximately 25% smaller.

The phase variations introduced by the klystron can be compensated using a phase shifter but this would require a combination of a very accurate feed-forward and feed-back phase compensation over a large output range which would improve the maximum energy in the cavity with less than 5%. Since the improvement of implementing such a system is very small and because of the difficulties of implementing a feed-forward and feed-back system it is not advisable to build such a controller. The total phase-jitter can be reduced by approximately 25% when using only feed-forward compensation to reduce the phase variation at maximum electric field inside the cavity, which reduces the phase jitter caused by the synchronization jitter between the modulator and the RF-signal phase. A larger reduction can be obtained by improving the stability of the high voltage power source.

Contents

Chapter 1

Introduction

1.1 Acceleration of short electron bunches.

Extremely short sub-picosecond electron bunches that contain a large number of electrons and have 'laser-like' properties (high brightness) are of interest to a number of disciplines. One of the applications is the creation of pulsed X-ray radiation. Until now the main route to create these short bunches has been to start with rather long bunches (on the picosecond timescale) and use magnetic compression after acceleration to higher energies. The advantage of this method is that the space-charge influences on the quality of the bunches, which is particularly severe at low energies, is avoided. This method, however, is not suited to create very short bunches (approximately $100fs$) because the electrons in the bunch start to radiate collectively in the bending magnets and this spoils the quality of the beam exiting the magnetic compressor.

An alternative to magnetic compression is to start with short bunches and keep them short during acceleration, thus avoiding the need of compression. Very short laser pulses (approximately $35fs$) can be used to create the short bunches. These bunches have to be accelerated to high energies within very short distances to maintain the high brightness of the beam. In order to attain beam characteristics as mentioned above, the acceleration field has to be at least $500MV/m$ which is far beyond the maximum attainable fields in state-of-the-art Radio Frequency (RF) accelerators. However, studies on vacuum breakdown indicate that metals can withstand voltage gradients of a few GV/m if the duration of the field is in the order of ns.

The highest voltage that can be switched on the ns timescale is in the order of $1MV$. Therefore a device is being developed, at Eindhoven University of Technology, for this project which should create approximately $2.5MV$ pulses with a pulse duration of approximately $1ns$. This is not enough to maintain the high brightness of the electron bunch so a second acceleration stage is needed to boost the energy to the $10MeV$ level which is enough to maintain the high beam quality. As most of the beam blow-up will occur at low velocities the requirements on the acceleration field in this second stage are less severe. Therefore it can be a state-of-the-art high field RF booster capable of maintaining the high quality of the beam.

At Eindhoven University of Technology a project has been started to build such a combined DC/RF accelerator. The experimental setup is schematically depicted in figure 1.1. Part of the actual setup is shown in figure 1.2.

At the left of figure 1.1 the electrons are created by a laser-pulse of approximately $35fs$ (a

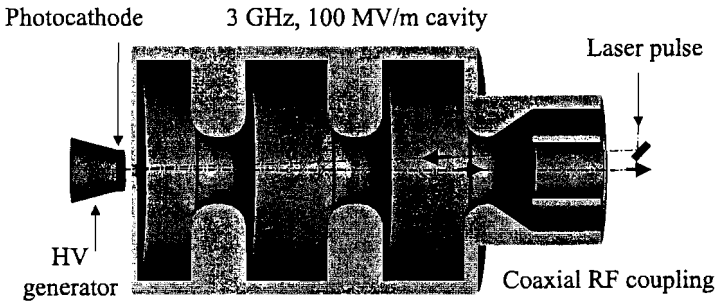

Figure 1.1: Experimental setup (schematically)

process which is called photo-emission). The high voltage pulse of approximately a nanosecond is synchronized with the laser-pulse. Since the laser pulse which creates the electrons is much shorter than the high voltage pulse the electrons are essentially accelerated in a DC field of $1GV/m$ to an energy of $2MeV$. After the first acceleration the electron-bunch enters an RF cavity trough a small hole. This cavity is an RF coupled resonant structure which creates a longitudinal electric field of standing waves (along the axis of the cavity). The length of each cell in the cavity has been chosen in such a way that the field changes sign when the electron bunch leaves one cell and enters the next. Using this principle the electrons are accelerated further to a final energy of $10MeV$.

For optimal acceleration the electrons have to start at the right phase of the RF field. In order to achieve this the laser pulses have to be synchronized to the RF signal. Usually this is done by synchronizing the laser to a fixed oscillator. In this setup a different approach is used. By using a $3GHz$ RF voltage controlled oscillator it is possible to synchronize the oscillator to the laser-pulses with less than $20fs$ time-jitter. This can be achieved because the control bandwidth can be increased from approximately $1kHz$ to $100kHz$ because the bandwidth of the oscillator is much larger ($10MHz$) than the bandwidth of the laser [K+01].

The RF cavity is filled with energy by a pulsed klystron tube (which is an RF amplifier just like for instance a magnetron). In order to fill the cavity this RF power pulse has to be

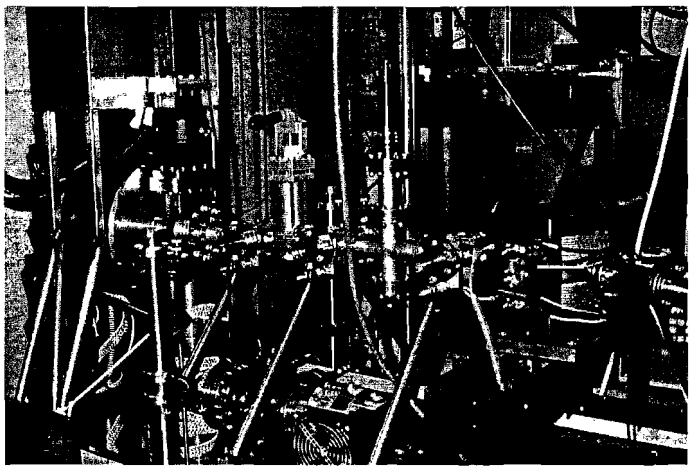

Figure 1.2: Picture of the experimental setup

approximately $4\mu s$ long. To create an RF power pulse the power input of the klystron tube is pulse modulated (the modulation device is called a modulator in the rest of this document). The modulator creates a pulse of approximately $20MW$ with a duration of $4\mu s$. The RF power pulse coming out of the klystron has a peak power of approximately $10MW$.

1.2 Problem definition.

Usually the modulator is designed to deliver a flat top power pulse. This is done by using a pulse forming network, containing a lot of high voltage capacitors and inductors, which simulates a long line. In the setup which is built at Eindhoven University of Technology a different approach is used. Instead of using a modulator creating a flat top pulse the modulator was designed to create an "exponentially shaped" pulse. The reasons for choosing an "exponentially shaped" pulse instead of a flat top pulse are:

- only one short electron bunch is accelerated per RF power pulse (which consumes only a very small fraction of the power) so there is no need for a constant output power.
- the modulator becomes very compact because it contains less large high voltage and high power components.
- the modulator becomes more reliable mainly because it contains less capacitors.
- the modulator becomes cheaper.

However there are problems connected with using an "exponentially shaped" pulse to power the klystron tube. Firstly the tube introduces a frequency change. This is caused by the changing acceleration voltages in the klystron which causes the output frequency of the klystron tube to shift with respect to its input frequency. Since the RF accelerator cavity has an extremely small bandwidth the changing delay causes the cavity to be shifted off resonance which means that the maximum RF field in the cavity will be smaller.

The second problem is that because of the changing frequency the phase of the RF field inside of the cavity will have a small time-dependency which could increase the phase jitter between the laser and the RF field inside the cavity. This might spoil the stability of the accelerator.

The third problem is caused by the shape of the pulse itself. Since the cavity has a very high quality factor it has a limited bandwidth which prevents it from reaching its maximum (steady state) value. This also results in a decrease of the maximum RF field inside the cavity.

1.3 Contents of this document

In this document the disadvantages of using an "exponentially shaped" pulse (described above) are analyzed. Chapter 2 contains the modelling of the process. It also contains an introduction which presents the basic theory necessary to analyze the problem. Chapter 3 contains the model evaluation using the measurements done on the system. Chapter 4 shows the final analysis of the problems presented in the problem definition using the simulation models of chapter 2 and by using the measurements of chapter 3. Chapter 5 contains the conclusions using the results of chapter 4 and it also contains recommendations for further study.

Chapter 2

Modelling

2.1 Introduction

In order to calculate the effect of the "exponentially shaped" modulator pulse on the field inside the cavity it is important to have a good model of the total process. This process can be divided into three main elements:

- the modulator.
- the klystron tube.
- the accelerator cavity.

The modulator generates a, high voltage, power pulse which is converted into RF power by the klystron tube. This RF power is fed into a resonant RF structure (the RF cavity) in order to setup an acceleration field. Unfortunately the impedance of the klystron is non-linear. This means that the resulting differential equations which describe the behavior of the modulator have to be solved numerically. By using the simulation models it is also possible to use measured data to validate the simulations.

This chapter describes the modelling necessary to calculate/simulate the process as shown in figure 2.1. Before describing all the different subsystems in detail, it is necessary to give a problem definition and at the same time explain our approach to the description of the process. The modulator, which is generating the power delivered to the power-input of the klystron, generates an "exponentially shaped" modulator-voltage pulse U_{mod}. The RF-output of the klystron is described by the resonance frequency ω_0 and the delay Δt:

$$U_{kly}(t;\omega_0) = f(U_{mod}(t))cos(\omega_0(t + \Delta t(t))) \tag{2.1}$$

Because the variation of the delay during one RF-period is very small it is possible to describe this delay as a instantaneous (time-dependent) RF-phase difference $\phi(t)$ between the RF-input and the RF-output of the klystron. The time dependent variation of this phase-difference can be described by an instantaneous frequency deviation $\omega_{det}(t) = \frac{d\phi(t)}{dt}$ resulting in:

$$U_{kly}(t;\omega_0) = f(U_{mod}(t))cos(\omega_0 t + \phi(t)) = f(U_{mod}(t))cos(\omega_0 t + \int \omega_{det}(t)dt + \phi_0) \tag{2.2}$$

The reasons for choosing an instantaneous frequency deviation are;

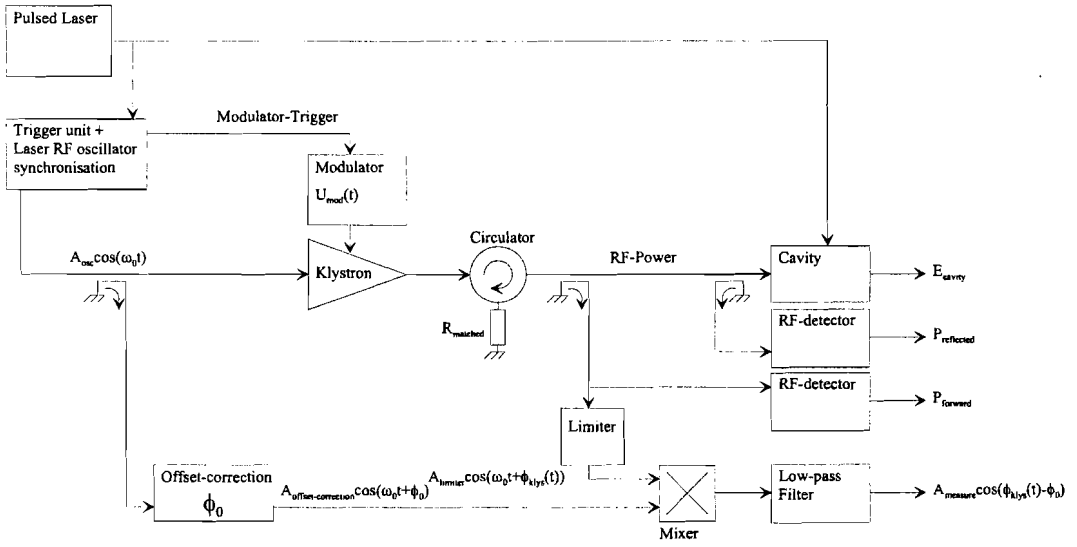

Figure 2.1: The block diagram of the process

- It provides a much more intuitive approach to the problem (which is described below);
- It is possible to measure the instantaneous phase difference by using a mixer as shown in figure 2.1; and
- It saves a lot of simulation bandwidth (which is described in section 2.4).

The instantaneous frequency deviation $\omega_{det}(t)$ is an undesired effect as it causes the cavity (which is a resonant structure with a very high quality factor) to be shifted off resonance. When the cavity is shifted off resonance it will not be filled optimally. This results in a smaller accelerating field and a larger phase jitter between the laser pulses and the RF-phase inside the cavity. Each section of this chapter describes a different component of the circuit.

2.2 The power modulator model

This section describes the derivation of the power modulator model. The power modulator is used to provide the pulsed input power to the klystron amplifier tube. Figure 2.2 gives the (simplified) power modulator circuit for generating the power pulse. The input voltage $U_{step}(t)$ is described by equation 2.3 where U_{HV} comes from a switched DC high voltage source and $\varepsilon(t)$ is the unit step function.

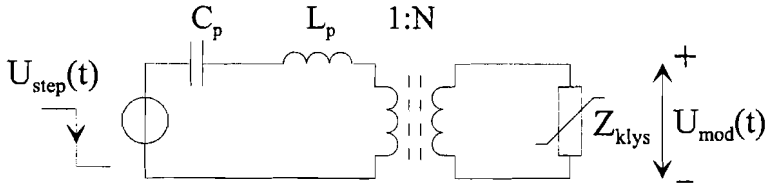

Figure 2.2: The power modulator circuit

$$U_{step}(t) = U_{HV}(1 - \varepsilon(t)) \tag{2.3}$$

The voltage pulse coming out of the modulator is a negative pulse. In the analysis of the klystron model the charge of electrons is assumed to be positive to simplify the calculations. This has no effect on the process but the modulator voltage pulse has to be positive. In the rest of this document the pulse will be assumed positive.

When the transformer is assumed to be ideal (and the voltage pulse is assumed to be positive) it is possible to use the equivalent circuit as shown in figure 2.3. This model can also include the leakage induction of the transformer since it can be added to the inductance of the modulator. The components shown in figure 2.2 are transformed to the secondary side of the transformer by equations 2.4 to 2.6.

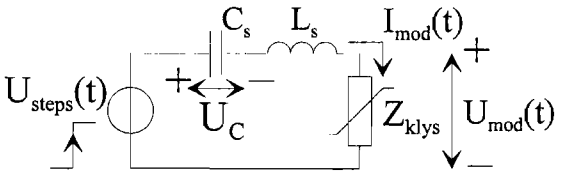

Figure 2.3: The transformed power modulator circuit

$$C_s = \frac{C_p}{N^2} \tag{2.4}$$

$$L_s = N^2 L_p \tag{2.5}$$

$$U_{steps}(t) = N U_{HV} \varepsilon(t) \tag{2.6}$$

The klystron input load Z_{klys} is non-linear. It is given by the "Child-Langmuir three-halves power law". Equation 2.7 shows the relation between the input current and voltage of the klystron where K $[AV^{-3/2}]$ is the perveance.

$$I_{mod} = K U_{mod}^{\frac{3}{2}} \tag{2.7}$$

First the solution of the modulator voltage is given by assuming a constant klystron load R_{eq} to show the behavior of the circuit analytically. In the laplace domain the circuit can be represented by a standard second order notation (equation 2.10) where ω_n (the natural frequency) and ζ (the damping ratio) are described by equations 2.8 and 2.9. Equation 2.11 describes the modulator signal as a function of time (under the conditions $\zeta > 0$ and $\zeta \in \mathbb{R}$). Equation 2.11 shows that the modulator output voltage, using a constant load, is described by an exponentially damped signal.

$$\omega_n = \frac{1}{\sqrt{L_s C_s}} \tag{2.8}$$

$$\zeta = \frac{R_{eq}}{2 L_s \omega_n} = \frac{R_{eq}}{2} \sqrt{\frac{C_s}{L_s}} \tag{2.9}$$

$$U_{mod}(s) = 2\zeta\omega_n U_{HV} \frac{1}{s^2 + 2\zeta\omega_n s + \omega_n^2} \tag{2.10}$$

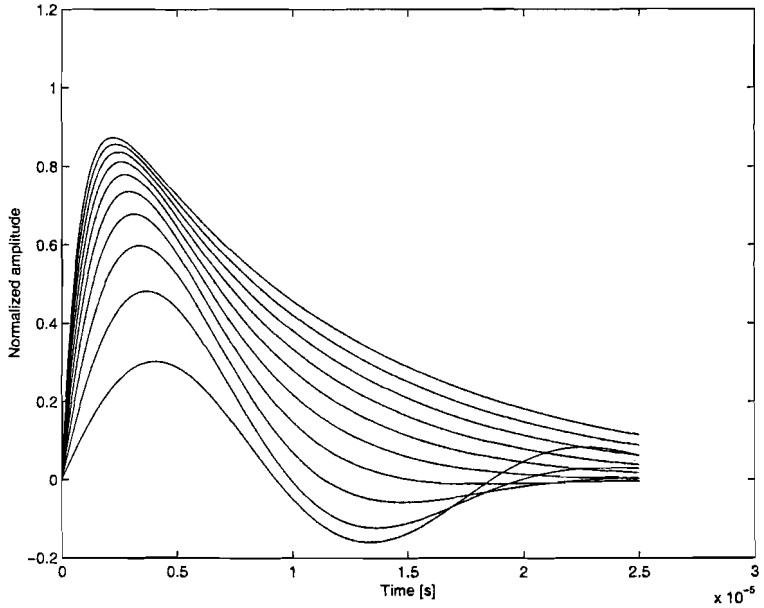

Figure 2.4: Normalized amplitude time response using various ζ values

$$U_{mod}(t) = \left\{ \begin{array}{ll} NU_{HV}\frac{2\zeta}{\sqrt{1-\zeta^2}}e^{-\zeta\omega_n t}\sin\left(\sqrt{1-\zeta^2}\omega_n t\right)\varepsilon(t) & ,0<\zeta<1 \\ NU_{HV}2\omega_n t e^{-\omega_n t}\varepsilon(t) & ,\zeta=1 \\ NU_{HV}\frac{\zeta}{\sqrt{\zeta^2-1}}\left(e^{-\omega_n\left(\zeta-\sqrt{\zeta^2-1}\right)t} - e^{-\omega_n\left(\zeta+\sqrt{\zeta^2-1}\right)t}\right)\varepsilon(t) & ,\zeta>1 \end{array} \right\} \tag{2.11}$$

$$\omega_n = \left\{ \begin{array}{ll} \frac{\arctan\left(\frac{\sqrt{1-\varsigma^2}}{\varsigma}\right)}{t_{maxU}\sqrt{1-\varsigma^2}} & ,0<\varsigma<1 \\ \frac{1}{t_{maxU}} & ,\varsigma=1 \\ \frac{\ln\left(\frac{\varsigma+\sqrt{\varsigma^2-1}}{\varsigma-\sqrt{\varsigma^2-1}}\right)}{t_{maxU}2\sqrt{\varsigma^2-1}} & ,\varsigma>1 \end{array} \right\} \tag{2.12}$$

Figure 2.4 shows the modulator voltage as a function of time when attached to a constant load for various values of ζ. When ζ is smaller than 1 the function behaves like an exponentially damped sinusoidal. When ζ increases above 1 the function becomes a double exponential signal. The damping of the linear system was set to approximately $\frac{1}{2}\sqrt{2}$ during the design of the modulator which is a tradeoff between the pulse height and pulse width and the maximum output voltage when considering the linear case. The actual modulator component values are given by table 2.1 (where L_p is the sum of the modulator inductance and the effective leakage inductance of the pulse transformer). The reason for lowering the damping ratio is explained at the end of this section. Table 2.1 also shows two linear approximations of the modulator circuit.

Approximation 1 uses the same component values as the non-linear version but it uses an equivalent constant load. This results in a approximation with the same maximum voltage (depending only on U_{HV} and ζ) but at the wrong time. This approximation provides the best linear equivalent constant load. Approximation 2 adapts the capacitor too in order to correct for the time difference (by adapting ω_n according to equation 2.12). This approximation is

Table 2.1: Component values.

Real Parameter	Value	
ζ	>0.66	
ω_n	0.324	$M\frac{rad}{s}$
L_p	19.0	μH
C_p	0.5	μF
N	13	
K	1.75	$\mu\frac{A}{V^{\frac{3}{2}}}$
Linear Approximation 1	Value	
ζ_{eq}	0.56	
R_{eq}	1.16	$k\Omega$
Linear Approximation 2	Value	
ζ_{eq}	0.56	
ω_{neq}	0.329	$M\frac{rad}{s}$
R_{eq}	1.18	$k\Omega$
C_{peq}	0.49	μF

more accurate but the values of the approximation do not tell much about the real parameters of the non-linear situation. The equivalent resistance is slightly smaller than the non-linear resistance at maximum voltage. Since the system is non-linear the load varies as a function of time. Using equation 2.7 it is possible to derive a set of differential equations (using the voltage across the capacitor U_C as a solving variable to avoid numerical problems when simulating the equations).

When equation 2.7 is used for the klystron load instead of the constant load the differential equations become non-linear and can only be solved numerically. Using equations 2.13 to 2.16 it is possible to simulate the non-linear behavior of the modulator as a function of time.

$$\frac{d^2U_C(t)}{dt^2} = \frac{1}{L_sC_s}\left(U_{steps}(t) - U_C(t) - K^{-\frac{2}{3}}C_s^{\frac{2}{3}}\left(\frac{dU_C(t)}{dt}\right)^{\frac{2}{3}}\right) \tag{2.13}$$

$$I_{mod}(t) = C_s\frac{dU_c(t)}{dt} \tag{2.14}$$

$$U_{mod}(t) = K^{-\frac{2}{3}}I_{mod}^{\frac{2}{3}}(t) \tag{2.15}$$

$$P_{mod}(t) = K^{-\frac{2}{3}}I_{mod}^{\frac{5}{3}}(t) \tag{2.16}$$

The implementation of the differential equations in the matlab simulink environment (which is used to simulate the problem) is shown in figure 2.5. There is one extra output added to the system. This output creates the dU_{mod}/dt signal necessary for simulating the instantaneous frequency deviation in the klystron simulink block (figure 2.10) which is explained in section 2.3 of this chapter. The solution of differential equations 2.13 to 2.16 resembles the exponentially damped sinusoidal of the linear case. The damping factor can also be calculated for the non-linear case using equation 2.9. Although ζ does not apply to the non-linear situation the calculated ζ still gives a good indication of the behavior of the non-linear process. Figure 2.6 shows the damping factor ζ of the non-linear system as a function of time when using

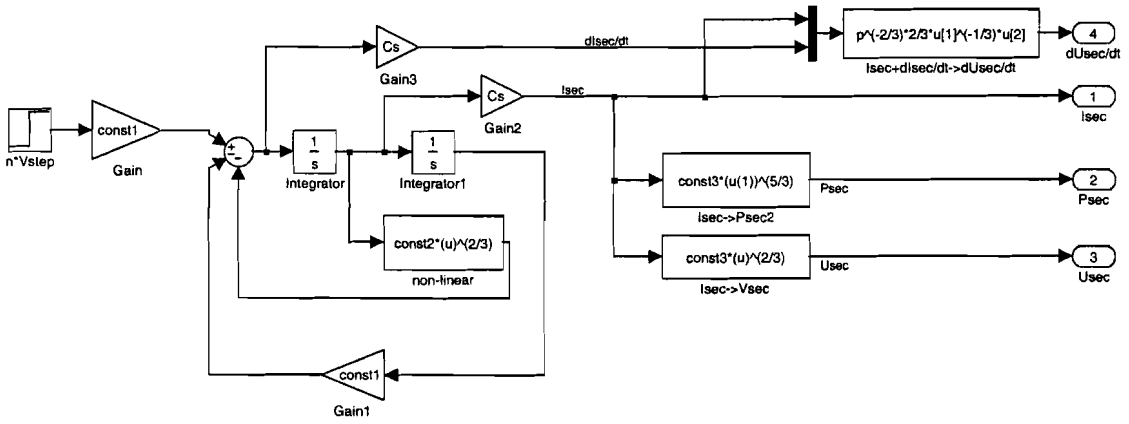

Figure 2.5: Layout of the "modulator" simulink model.

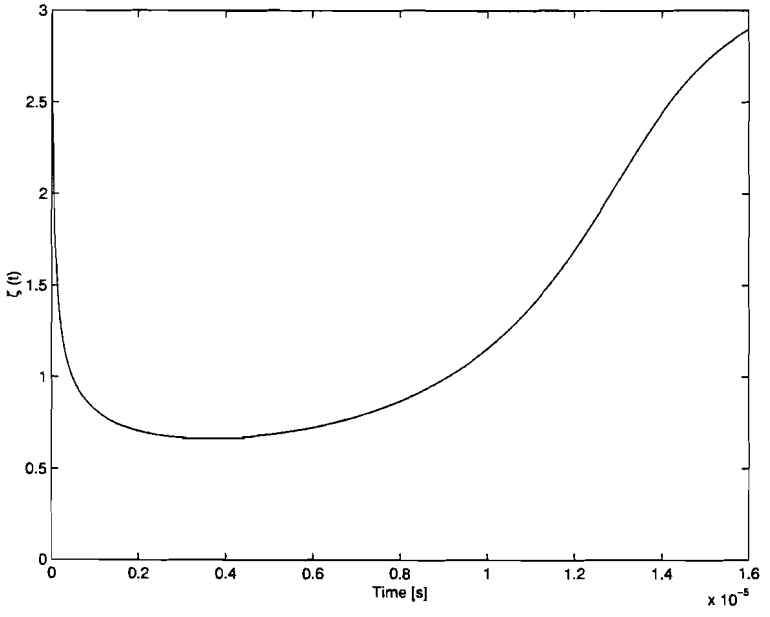

Figure 2.6: ζ as a function of time

the actual step height. The damping factor ζ has become time dependent (and slightly input voltage dependent) because of the voltage dependency of the load.

Figure 2.7 shows the linearized approximation (number 2 from table 2.1) and the non-

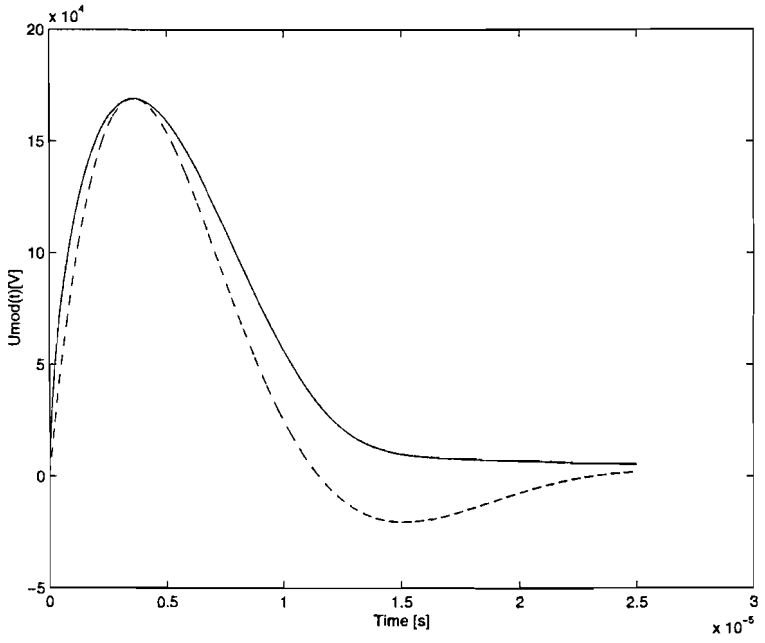

Figure 2.7: Linear and non-linear modulator voltage as a function of time

linear voltage simulation of the modulator system at the actual settings. In the first part of the modulator pulse the system behaves like a double exponential function ($\zeta > 1$) at maximum the system behaves like an exponentially damped sinusoidal ($\zeta < 1$) and at the last part of the simulation the system again starts behaving like a double exponential function. Because of the resemblance with the linearized pulse the non-linear pulse coming out of the modulator is called an "exponentially shaped" modulator pulse in the rest of this document. Since the pulse width has to be large enough for the cavity to fill with energy it is better to lower the damping factor to a smaller value, which increases the pulse width of the modulator output pulse (as can be seen from the linear case shown in figure 2.4). In the linear case the modulator output signal would start to behave like an exponentially damped sinusoidal signal but since the nonlinearity of the load increases the damping factor when the voltage on the load decreases as can be seen from picture 2.6 (the dashed line shows the linearized version and the solid line shows the non-linear version) the system will still be normally damped. The lower maximum output voltage resulting from lowering the damping factor can be compensated by increasing the voltage on the high voltage supply.

2.3 The Klystron model

A klystron is an amplifier for microwave signals. It consists of a vacuum tube in which an electron beam is created. The tube consists of four basic parts (which are shown in figure 2.8);

- 1 The acceleration part

- 2 The modulation part
- 3 The drift space
- 4 The generation part

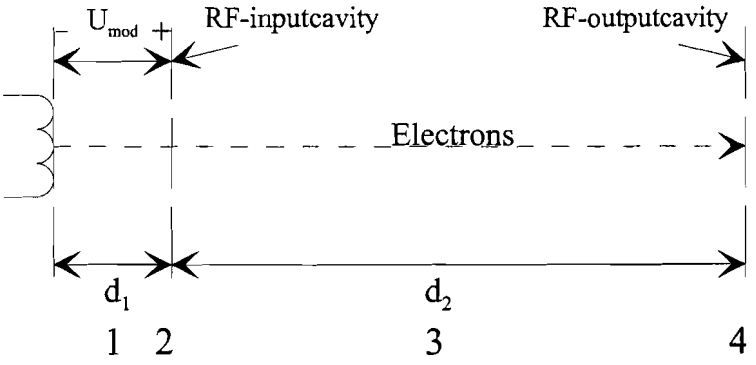

Figure 2.8: The klystron model

In the acceleration part the electrons created at the cathode are accelerated using the modulator voltage. Subsequently the electron beam is velocity modulated by the RF input power while traversing the RF input cavity (the modulation part). In the drift space the faster particles overtake the slower particles creating a modulated distribution of charge. This process is called bunching and it can be used for power amplification of high frequencies. In modern klystrons the drift space contains several additional cavities to improve the gain, efficiency and bandwidth of the klystron. The output power of the klystron amplifier is generated at the output cavity (the generation part).

An accurate large signal analysis of the output power as a function of the input power of a modern high efficiency klystron would require all the dimensions of the klystron tube and a 2-D or 3-D space charge model. It is possible however to derive an analytic expression describing the influence of the first cavity (or modulating cavity) on the beam of the klystron. Since the other cavity's are used to optimize the efficiency, gain and bandwidth of the klystron the influence of the first cavity gives a qualitative estimate of the beam current behavior at the output cavity. The amplitude of the fundamental current component of the velocity modulated beam at a distance d_2 with an initial velocity v_e and an initial velocity modulation depth α is given by equation 2.19 where $J_1(x)$ is a Bessel function of the first kind and x is the (normalized) bunching parameter which is given by equation 2.18 (M is the beam coupling factor).

For more information about klystron theory please read [Sla50] and [SP95]. The bunching parameter given by equation 2.18 is only valid for non-relativistic calculations. When the initial velocity approaches the speed of light the modulating effect will also decrease. The correction factor on the beam coupling for the relativistic case is given by 2.20 where γ is the total electron energy normalized to m_0c^2 (which is explained in section 2.3.2 and given by equation 2.27). The correction on the beam coupling factor is calculated using the method of calculating the bunching parameter given by [Sla50] starting with the relativistic energy balance instead of the non-relativistic one.

$$\alpha = \frac{U_{rf-in}}{U_{mod}} \tag{2.17}$$

$$x = \frac{1}{2}\frac{\alpha M \omega_0 d_2}{v_e} \tag{2.18}$$

$$I_{beam} = 2I_{mod}J_1(x)\sin\omega_0\left(t - \frac{d_2}{v_0}\right) \tag{2.19}$$

$$M_{rel} = \frac{2}{\gamma(\gamma+1)}M \tag{2.20}$$

The klystron tube which is used in the system is a Thomson TH2157 S-band tube which is modified by the manufacturer to deliver a $10MW$ output pulse. The only provided specification of the klystron output power is given in the form of a power efficiency factor μ at nominal output power which is 49%. This is an extremely high value since the theoretical maximum lies at 50%. The output function of the tube has been measured and can be found in section 3.3.1.

The emphasis in this document is on analyzing the phase behavior of the cavity so it is more important to have an accurate phase model than a model describing the exact amplitude. This chapter describes the derivation of a model suited for calculation and/or simulation of the phase-difference between the input and output cavity of the klystron amplifier as a function of the modulating voltage. In section 2.3.1 calculations are done for the non-relativistic case. Section 2.3.2 contains the same calculations when corrected for the relativistic effect. The derivation of the non-relativistic equations is included because they are much easier and they help to understand the relativistic equations.

Because the modulator, which generates the power delivered to the power-input of the klystron, generates an "exponentially shaped" modulator-voltage pulse U_{mod}, the initial speed v_e of the klystron beam, and thus the delay between the RF-input and RF-output of the klystron, will vary during the pulse:

$$U_{out}(t;\omega_0) = f(U_{mod}(t))cos(\omega_0(t + \Delta t(t))) \tag{2.21}$$

Because the variation of the delay during one RF-period is very small it is possible to describe this delay as an instantaneous (time-dependent) RF-phase difference $\phi(t)$ between the RF-input and the RF-output of the klystron. For a small modulation index α (equation 2.17) the instantaneous phase difference between the RF-input and the RF-output of a klystron ϕ can be modelled by assuming a travelling wave with a constant speed v_e and a frequency ω_0 travelling a distance d_2 between the input-cavity and the output-cavity of the klystron (figure 2.8 and equation 2.22).

$$\phi(t) = \frac{d_2\omega_0}{v_e(t)} \tag{2.22}$$

The variation of this phase-difference can be described by an instantaneous frequency deviation $\omega_{det}(t) = \frac{d\phi(t)}{dt}$:

$$U_{out}(t;\omega_0) = f(U_{mod}(t))cos(\omega_0 t + \phi(t)) = f(U_{mod}(t))cos(\omega_0 t + \int \omega_{det}(t)dt + \phi_0) \tag{2.23}$$

2.3.1 Frequency deviation using non-relativistic particles

It is possible to derive a formula which calculates the instantaneous frequency deviation $\omega_{det}(t)$ as a function of the modulator-voltage U_{mod} by solving the energy balance resulting in equations 2.24 and 2.25. The derivation of equations 2.24 and 2.25 is included in appendix

A. Both equations are only valid when the transition time $t_{tr}(t)$ [s], of the electrons travelling a distance d_1 from the cathode to the input-cavity of the klystron, is neglected. Since the assumption $t_{tr} = 0$ can only be made when $U_{mod}(t)$ is assumed to be constant during the acceleration of the electrons (on the interval $[t_{z=0}, t_{z=d_1}]$) the outcome of equations 2.24 and 2.25 are slightly inaccurate for simulating the modulator-pulse for small values of U_{mod}.

$$\omega_{det}(t) = -\frac{\omega_0 d_2}{v_e(t)} \frac{1}{U_{mod}(t)} \frac{1}{2} \frac{dU_{mod}(t)}{dt} \tag{2.24}$$

$$= -\frac{\omega_0 \cdot d_2}{2\sqrt{\frac{2q}{m_0}} U_{mod}^{3/2}(t)} \frac{dU_{mod}(t)}{dt} \tag{2.25}$$

In order to correctly simulate the instantaneous frequency deviation $\omega_{det}(t)$ for large values of $\frac{dU_{mod}(t)}{dt}$ at small values of $U_{mod}(t)$ it is necessary to include the transition time $t_{tr}(t)$. This complicates the calculations because the velocity has to be calculated using the complete contribution of the modulator voltage during the interval $[t_{z=0}, t_{z=d_1}]$. In order to check whether or not to use the simple model, the model including the transition time is simulated by using the set of differential equations derived in appendix B. Since the non-relativistic approach is included as an introduction to the problem before explaining the relativistic calculations the model evaluation is not done for the non-relativistic case. In the next section (2.3.2) a comparison is made between the model which includes the transition time and the model which ignores the transition time for the relativistic case.

2.3.2 Frequency deviation using relativistic particles

When using the non-relativistic electron velocity equation (2.26) the maximum speed v_{emax} becomes $v_{emax} \approx 2.44 \cdot 10^8$ m/s (calculated at a maximum U_{mod} of $169kV$).

$$v_e(t) = \sqrt{\frac{2qU_{mod}(t)}{m_0}} \tag{2.26}$$

The equations from section 2.3.1 are only valid when the speed v_e is much smaller than the speed of light $c \approx 3 \cdot 10^8$ m/s. Since this is not the case the phase-difference has to be calculated by taking into account the relativistic effects of particles travelling at a speed that approaches the speed of light. This is done in appendix 2.3.2 (a large part of this derivation can also be found in [P+91] but for a slightly different application). In order to simplify the equations $\gamma(t)$ is introduced which is the total electron energy normalized to m_0c^2 (equation 2.27). Equation 2.24 now changes into equation 2.28 and equation 2.25 changes into equation 2.29.

$$\gamma(t) = \frac{eU_{mod}(t)}{m_0c^2} + 1 \tag{2.27}$$

$$\omega_{det}(t) = -\frac{d_2\omega_0}{v_e(t)} \frac{1}{\gamma(t)(\gamma(t)+1)} \frac{1}{U_{mod}(t)} \frac{dU_{mod}(t)}{dt} \tag{2.28}$$

$$-\frac{d_2\omega_0}{c} \frac{1}{(\gamma(t)+1)\sqrt{\gamma^2(t)-1}} \frac{1}{U_{mod}(t)} \frac{dU_{mod}(t)}{dt} \tag{2.29}$$

Again Equations 2.28 and 2.29 do not include the transition-time $t_{tr}(t)$ of electrons travelling a distance d_1 from the RF-input cavity to the RF-output cavity of the klystron. When

including the transition-time the problem results in a set of differential equations which are derived in appendix D. In order to maintain causality of the simplified model the simulation starts at time $t_{tr}(t = t_{tr})$ which is the time it takes for the first electrons to cross the distance d_1 between the cathode and the input cavity. This is done because before that time there is no beam at the input cavity so there is no phase relation between the input and the output of the klystron. A simplified set of differential equations (equations 2.30 to 2.35) can be derived from the equations of appendix D to calculate this first transition time.

$$\beta(t) = \frac{v_{ze}(t)}{c} \tag{2.30}$$

$$z(t = 0) = 0 \tag{2.31}$$

$$\beta(t = 0) = 0 \tag{2.32}$$

$$\frac{d\beta(t)}{dt} = \frac{q}{d_1 m_0 c} U_{mod}(t) \left(1 - \beta^2(t)\right)^{\frac{3}{2}} \tag{2.33}$$

$$\frac{dz(t)}{dt} = c\beta(t) \tag{2.34}$$

$$t_{tr} = (t|z(t) = d_1) \tag{2.35}$$

Table 2.2: Comparing two simulation options.

	Ignoring transition time[1]	Including transition time
Simulation speed:	++	−−
Simulink implementation:	+	−
Accuracy:	−	+

It is useful to compare both calculation methods before choosing one of them. Table 2.2 shows a comparison of both methods. As seen from table 2.2 ignoring the transition time has some advantages except for the accuracy. In order to investigate the loss of accuracy both methods where implemented and simulated. The maximum relative velocity error (which is a good indication for determining the accuracy since it does not contain any singularities) between both simulation methods is given by figure 2.9. In the first part of the simulation the error is 12% but it rapidly converges to a velocity error smaller than 0.02%. Since the error of the simplified method is very small in the area of interest it is possible to use the simplified model. The implementation of the simplified model in Simulink is shown in figure 2.10.

2.4 The cavity model

In this section the model of a resonant cavity is discussed. The cavity used in the experiment has several resonant frequencies which are shown in figure 2.11. Since only one of the resonant frequencies shown in figure 2.11 is of interest, i.e. $\omega_0 = 2\pi \cdot 2.9985 \cdot 10^9 \frac{rad}{s}$, and the separation of the resonant frequencies is large enough not to spoil the simulations, it is possible to use an equivalent resonant RLC-circuit. When the matching of the RF power to the cavity impedance

[1]The transition-time $t_{tr}(t)$ [s] is the time it takes for the electrons to cross the distance between the cathode and the modulating cavity.

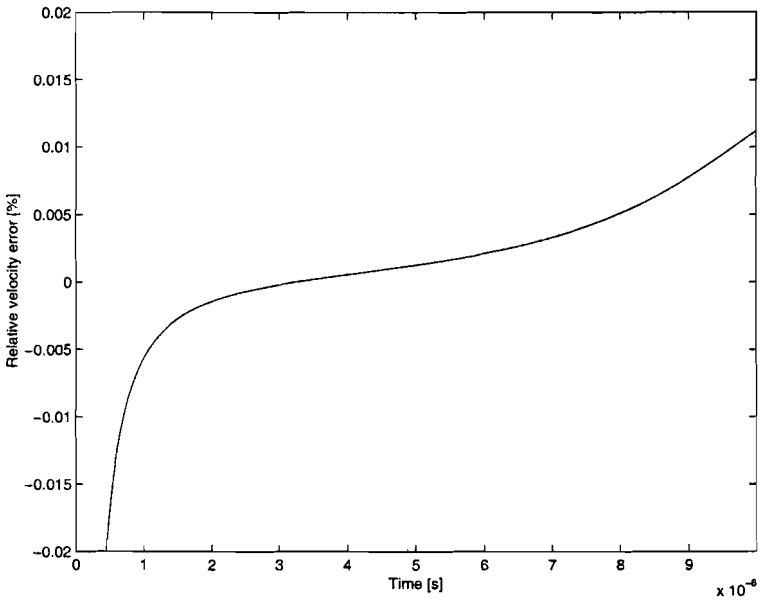

Figure 2.9: Relative error-percentage of the velocity simulation.

is ideal the absorption at resonance should be 100% but because of a small mismatch (0.01%) the reflection at resonance is equal to $-40dB$. Since the mismatch is very small the simulations in this document assume an ideal coupling between the RF power and the cavity.

Section 2.4.1 contains information about the parameters used to describe the resonant cavity. Section 2.4.2 contains information about the model that is used for simulation and also a short explanation of the "complex envelope theory". A more detailed explanation of this theory can be found in [Cou01].

2.4.1 The RLC-equivalent of the resonant cavity

The behavior of the resonant cavity can be modelled by using the resonant frequency $\omega_0 = 2\pi \cdot 2.9985 \cdot 10^9 \frac{rad}{s}$, the quality factor $Q = 14000$ and its resistance at resonance $R = 50\Omega$. The quality factor Q can be obtained by using its definition which is given by equation 2.36 where W_{tot} is the total average energy stored per cycle and P_{loss} is the dissipated power.

$$Q = \omega_0 \frac{W_{tot}}{P_{loss}} \tag{2.36}$$

The lumped circuit equivalent of the cavity is given by a parallel RLC-circuit (figure 2.12). The lumped circuit components can be converted to a Q factor and a resonant frequency ω_0 by using equations 2.38 and 2.37.

$$\omega_0 = \frac{1}{\sqrt{LC}} \tag{2.37}$$

$$Q = \frac{R}{\omega_0 L} \tag{2.38}$$

The cavity impedance Z_{cavity} as a function of ω is given by equation 2.40 (both notations). The amplitude and phase behavior of the cavity is shown in figure 2.13. The bandwidth of the cavity is shown by the distance between the two + markers in figure 2.13 which are placed

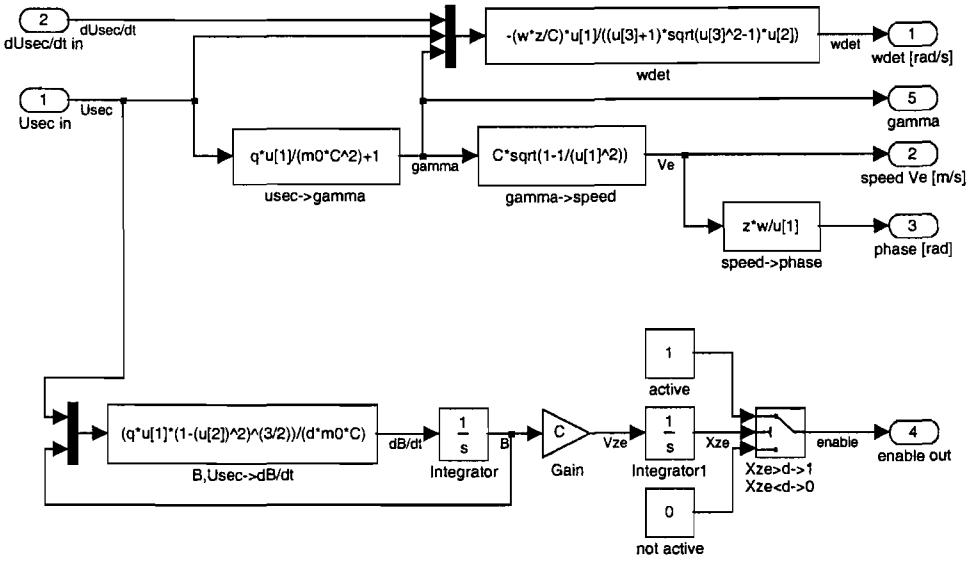

Figure 2.10: The klystron simulink model.

at $\frac{1}{2}\sqrt{2}$ of the maximum (this corresponds to $\frac{1}{2}$ the maximum power). The bandwidth is also given by equation 2.39.

$$BW = \frac{1}{Q} \tag{2.39}$$

$$Z_{cavity}(\omega) = \frac{U_c}{I_c}(\omega) = \frac{1}{\frac{1}{R} + j\omega C - j\frac{1}{\omega L}} = \frac{\frac{R}{Q}}{\frac{1}{Q} + j\left(\frac{\omega}{\omega_0} - \frac{\omega_0}{\omega}\right)} \tag{2.40}$$

The lumped circuit equivalent used for simulation of the resonant cavity is a loaded parallel RLC-circuit as shown in figure 2.14. The loaded RLC-circuit can also be described by the resonant frequency ω_0 [rad/s] but the quality factor of the loaded cavity is affected by the source impedance. Equations 2.41 to 2.43 show how to adapt the parameters of both equivalent circuits by introducing an external load R_e which results in an external quality factor Q_e. For optimal energy transfer the external source impedance matches the impedance of the cavity at resonance ($R = R_e$). The transfer-function of the cavity including the source impedance as a function of ω is given by equation 2.44 (both notations). The transfer-function of the loaded cavity is shown in figure 2.15.

$$R_l = R//R_e = \frac{R \cdot R_e}{R + R_e} \tag{2.41}$$

$$Q_e = \frac{R_e}{\omega_0 L} \tag{2.42}$$

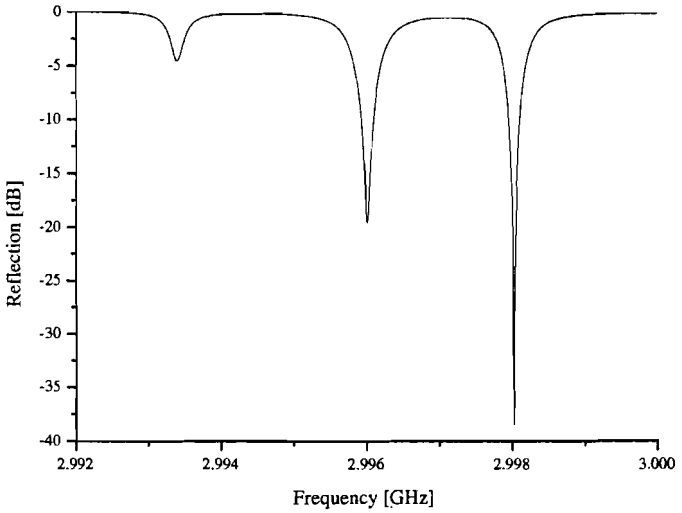

Figure 2.11: Measured absorption of the resonant cavity

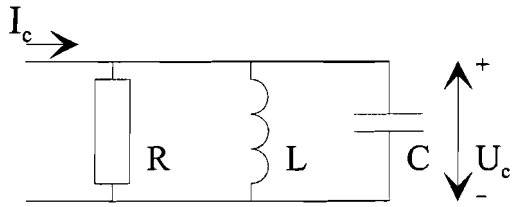

Figure 2.12: Lumped circuit equivalent of the cavity.

$$Q_l = Q//Q_e = \frac{Q \cdot Q_e}{Q + Q_e} \tag{2.43}$$

$$Z_l(\omega) = \frac{U_c}{I_k}(\omega) = \frac{1}{\frac{1}{R_l} + j\omega C - j\frac{1}{\omega L}} = \frac{\frac{R_l}{Q_l}}{\frac{1}{Q_l} + j\left(\frac{\omega}{\omega_0} - \frac{\omega_0}{\omega}\right)} \tag{2.44}$$

2.4.2 The complex envelope representation of the resonant cavity

The resonant frequency ω_0 is much larger than the instantaneous frequency deviation ω_{det}. It is very time consuming to simulate the behavior of the cavity by using the normal transfer function because it would require a simulation bandwidth ω_s [rad/s] given by equation 2.45.

$$\omega_s \geq 2(\omega_0 + \omega_{det\_max}) \tag{2.45}$$

Since the resonant frequency is a known and fixed parameter is it possible to simplify the model using a simplification called "complex envelope representation" (see [Cou01]). Using this theory it is possible to rewrite the "band-pass filter" transfer function of the resonant

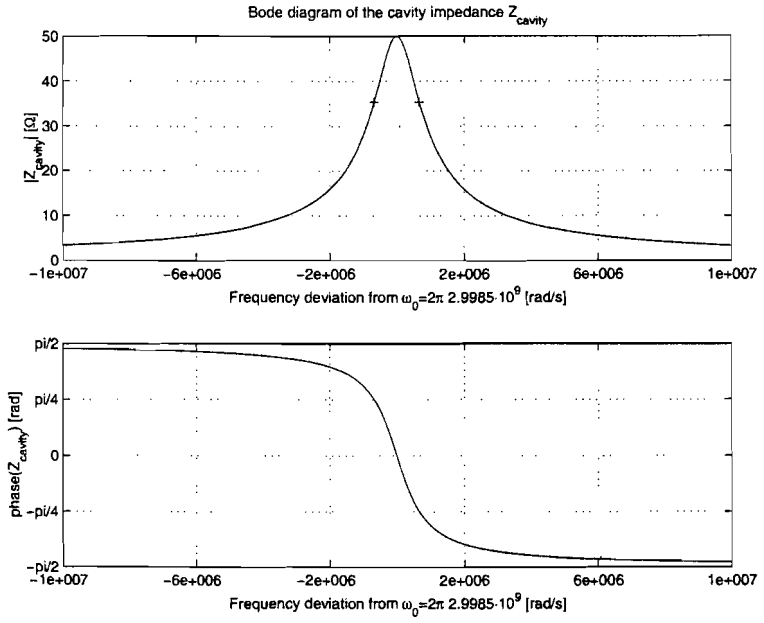

Figure 2.13: Bode plot of the cavity impedance

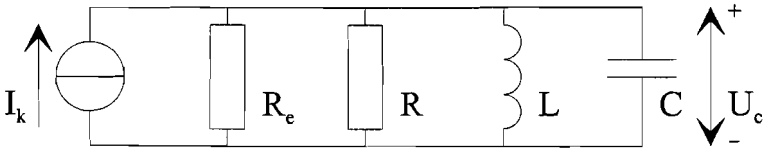

Figure 2.14: The lumped circuit equivalent of a loaded resonant cavity.

structure (figure 2.16) into an equivalent complex "low-pass filter" transfer function as shown in figure 2.17. In order to reduce the amount of variables, and to show the difference between the time domain and the frequency domain, the time domain variables are written in lower case and the frequency domain variables are written in upper case in this section. The advantage of using this theory is that it reduces the simulation bandwidth ω_s drastically as seen from equation 2.46.

$$\omega_s \geq 2(\omega_{det\_max} - \omega_{det\_min}) \tag{2.46}$$

Equation 2.47 gives the complex envelope representation of the resonant cavity as derived in appendix E.

$$K_Z(j\omega) = \frac{R_l\omega_0}{Q_l}\left\{\frac{1 + j\frac{1}{2Q_l\sqrt{1-\frac{1}{4Q_l^2}}}}{j\omega + \frac{\omega_0}{2Q_l}}\right\} \tag{2.47}$$

The input signal can be rewritten into a complex signal given by equation 2.48.

$$g_{i_k}(t) = |i_k(t)|\, e^{j\phi(t)} \tag{2.48}$$

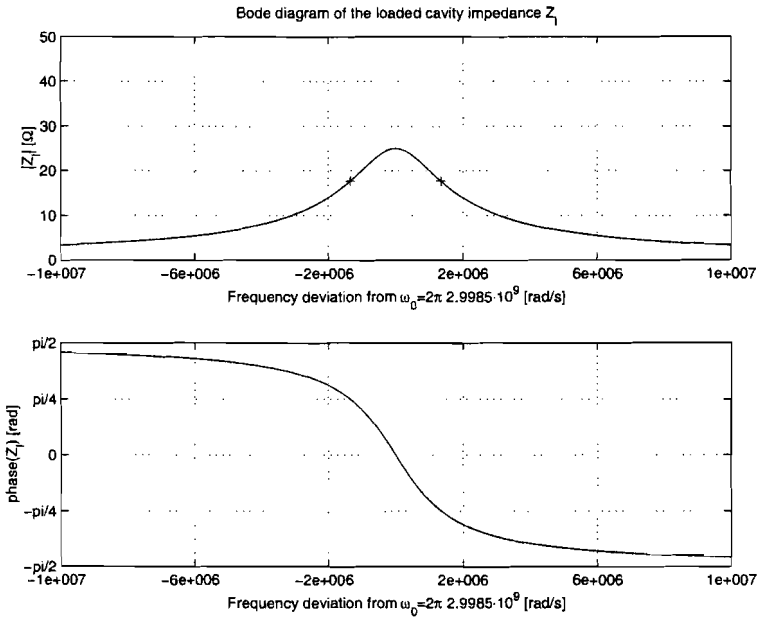

Figure 2.15: Bode plot of the loaded cavity

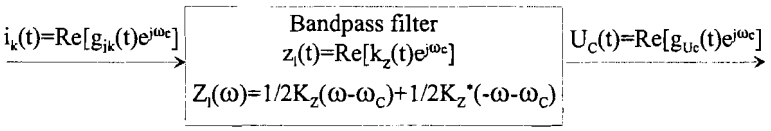

Figure 2.16: This is the "band-pass filter" notation of the resonant cavity.

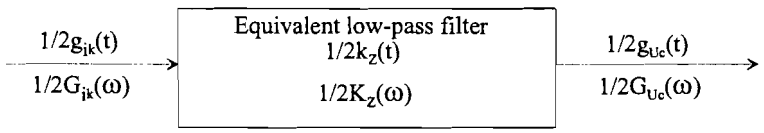

Figure 2.17: This is the equivalent "low-pass filter" notation of the resonant cavity.

Chapter 3

Measurements and model evaluation

3.1 Introduction

This chapter explains some of the less trivial measurement methods. It also contains the measured data derived from the experimental setup. The models derived in chapter 2 are evaluated using the measured data of the experimental setup. Section 3.2 contains an evaluation of the modulator model using the modulator measurement results. Section 3.3 contains the klystron measurements. Section 3.3 is divided into subsection 3.3.1, which contains the measurements of the klystron output power, and subsection 3.3.2, which contains the evaluation of the klystron phase model using the klystron output phase measurements. Section 3.4 contains a typical cavity power measurement.

3.2 Modulator measurements and model evaluation

In this section the modulator model derived in section 2.2 is compared with the measurements. The measurement where done using a high-voltage capacitive divider with an accuracy of 5% and a droop-rate of less then 0.02% per μs at the secondary side of the pulse transformer. Since there where uncertainties about the calibration accuracy of the capacitive divider, the modulator voltage measurements where calibrated by using the klystron power measurements improving the accuracy to 2.8% (which is explained in section 3.3.1 of this document).

Using the measured data it is possible to fit the simplified non-linear model (derived in section 2.2) to the measurement data resulting in figure 3.1. Figure 3.1 shows the measured modulator voltage (solid line) and the simulated modulator voltage (dashed line) at nominal operation for equal input voltages ($22.4kV$). The fit was made by assuming an equal input voltage at nominal operation ($22.4kV$) and placing the maximum of the pulse at the same height and time. The model describes the maximum output voltage accurately (less then 0.3% error) for the full measurement range of input voltages.

Figure 3.2 shows the measured modulator output voltage pulse as a function of time for increasing values of the input voltage. The used input voltages are: $U_{HV} = [\ 16.2kV, 16.7kV, 17.3kV, 17.9kV, 18.5kV, 19.0kV, 19.6kV, 20.2kV, 20.7kV, 21.3kV, 21.8kV, 22.4kV, 23.0kV, 23.6kV, 24.1kV\ ]$. As seen from figure 3.2 the pulse transformer produces a pulse whose shape can be described in first approximation by a "double exponential", as shown in figure 2.4.

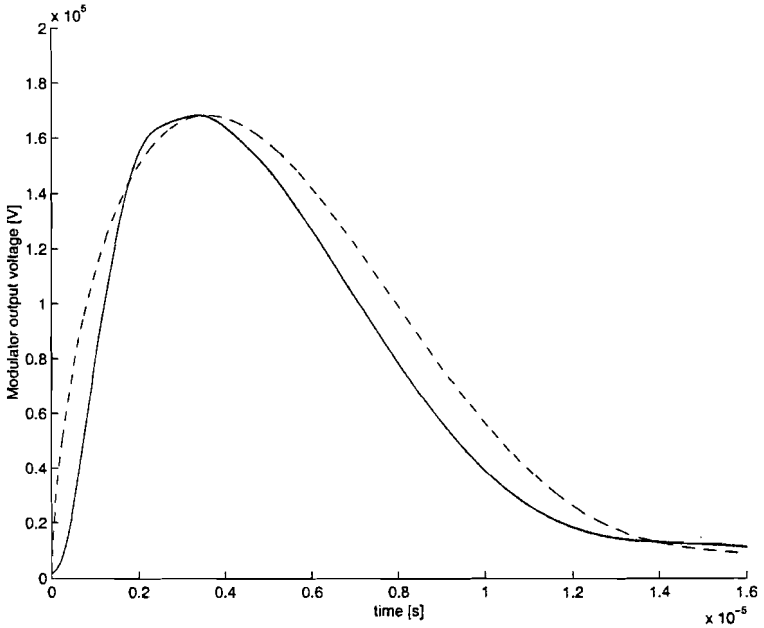

Figure 3.1: Measured modulator output voltage

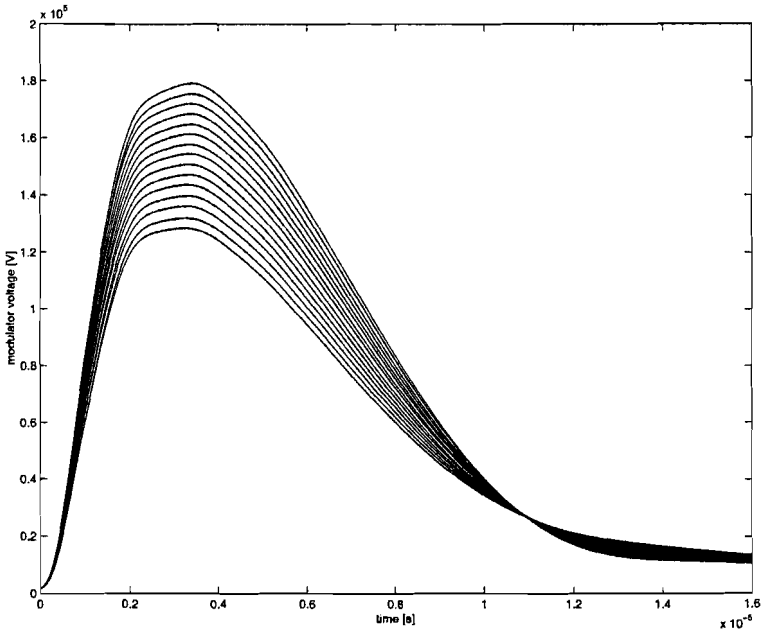

Figure 3.2: Measured modulator output voltage

However, the detailed behavior deviates from the "double exponential" shape. Just before the peak a flat slope is introduced, which is not present at the primary side of the pulse transformer. This flat slope cannot be explained by a simple lumped circuit model. The flat slope might be some hysteresis effect of the pulse transformer. The effect could be interesting to investigate further in order to increase the accuracy of the simulation model. Figure 3.3 shows the simulated pulse using the same input voltages that where used to measure the

modulator pulse.

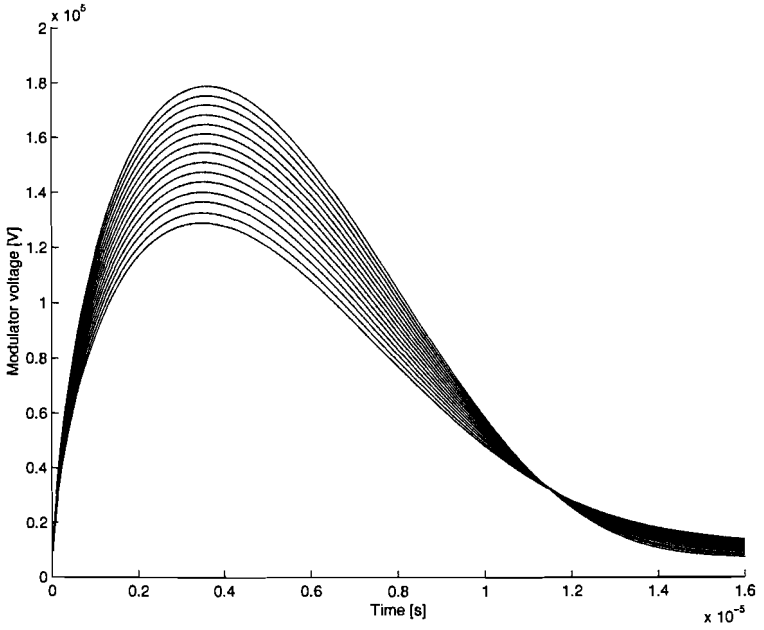

Figure 3.3: Simulated modulator output voltage

The flat slopes in the measured modulator pulse make it impossible to create a very accurate fit of the pulse shape necessary for the rest of the simulation. This is caused by the fact that the derivative of the modulator output voltage around maximum is very important for the accelerator cavity simulation. The derivative can be used to determine the phase variation at maximum power, which has the largest contribution to the total stored cavity energy. Since the phase measurements are very accurate it is possible to simulate the phase changes more accurately by using the measured data as an input for the phase simulations.

3.3 Klystron measurements and model evaluation

This section describes the measurements done on the klystron amplifier tube. Subsection 3.3.1 explains the power measurements and it also explains the calibration of the modulator voltage measurements. Subsection 3.3.2 explains the phase measurements.

3.3.1 Klystron power measurements

Because the output power of the klystron is an unknown function of the input voltage U_{mod} it is measured at different values of the input voltage. The power is measured by using a directional coupler which is built in the waveguide system at the output of the klystron. Since it is difficult to perform measurements near the experimental setup when the accelerator cavity is used (because of the radiation) the cavity has been replaced by a dummy load. This will not influence the measurement results because the output of the klystron is connected to the load by a circulator so the load impedance seen by the klystron is always matched to the source impedance of the klystron regardless of what is connected to the other side of the circulator. A small fraction of the RF output power ($-50.2dB$) is measured by a

directional coupler which is placed in the waveguide. This small fraction of the power is attenuated further ($-44.6dB$) to meet the specifications of the RF envelope detector which is connected to the system. It is very difficult to calibrate this measurement because the total attenuation of the system is very large and difficult to measure accurately. An RF power probe was sent to the 'NMI' (Nederlands Meet Instituut). This RF probe has been calibrated with an accuracy of 2%. Using the RF probe as a secondary measurement standard it has been possible to calibrate the RF components of the system resulting in a total accuracy of the power measurement of approximately 5%. Figure 3.4 shows the output RF-power of the klystron for various input voltages of the modulator (U_{HV} = [$16.2kV$, $16.7kV$, $17.3kV$, $17.9kV$, $18.5kV$, $19.0kV$, $19.6kV$, $20.2kV$, $20.7kV$, $21.3kV$, $21.8kV$, $22.4kV$, $23.0kV$, $23.6kV$, $24.1kV$]) and a klystron input RF-power of $60W$. The measured power is corrected for the losses in the circulator which are 5% so the actual power going into the cavity is 5% lower.

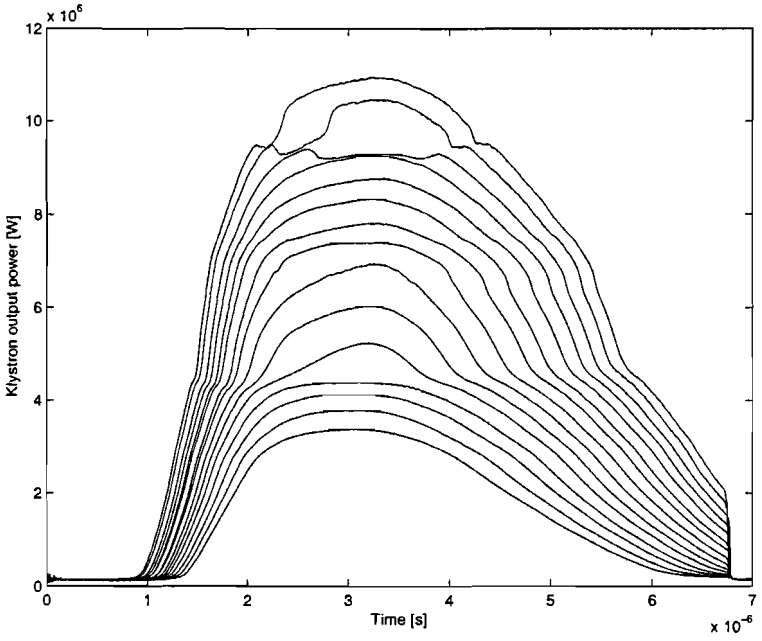

Figure 3.4: Measured klystron output power

The manufacturer of the klystron optimized the beam coupling and the cavity positions inside the klystron tube for optimal operation at a flat top output RF power-pulse of $10MW$. Since the pulse shape presented at the input of the klystron is exponentially shaped the klystron is excited over a large input voltage range (instead of using it at a fixed operating point). This means that the output power is sensitive to all possible misalignments of the klystron. One of the effects of misalignment is an oscillation visible on the output RF-power at approximately $4.5MW$ (which is also visible at the output phase). This oscillation is shown in figure 3.5. In order to reduce these oscillations the bunching parameter:

$$x = \frac{1}{2}\frac{\alpha M \omega_0 d_2}{v_e} \tag{3.1}$$

(see section 2.3) was slightly changed as explained below.

First the influence of the input RF-power on the output power was tested. It turns out that when the RF-power becomes too high the efficiency of the klystron tube decreases and

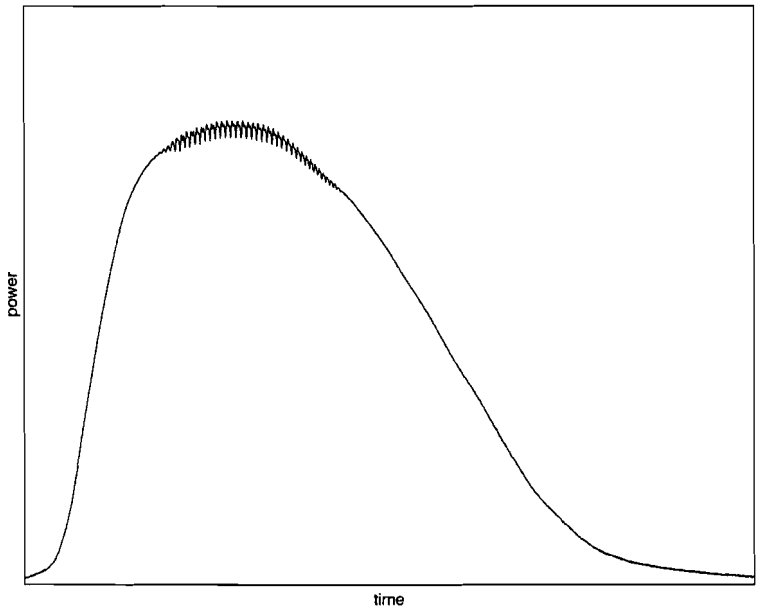

Figure 3.5: Oscillations on the output power

when it becomes too low the oscillations on the output power increase. The input power was set to $60W$ with an accuracy of approximately 5% by using fixed attenuators. This resulted in a $10MW$ pulse according to the specifications. The klystron has three focusing coils which are used to maintain the focus of the klystron beam. After optimizing the input RF-power, the current of the first focusing coil has been adjusted slightly, which changes the beam coupling coefficient M. The oscillations on the pulse shape are now much smaller in amplitude but the optimal output power is slightly lower than before. The output power also shows some inversion. The inversion is shown in figure 3.4 by the three highest power curves.

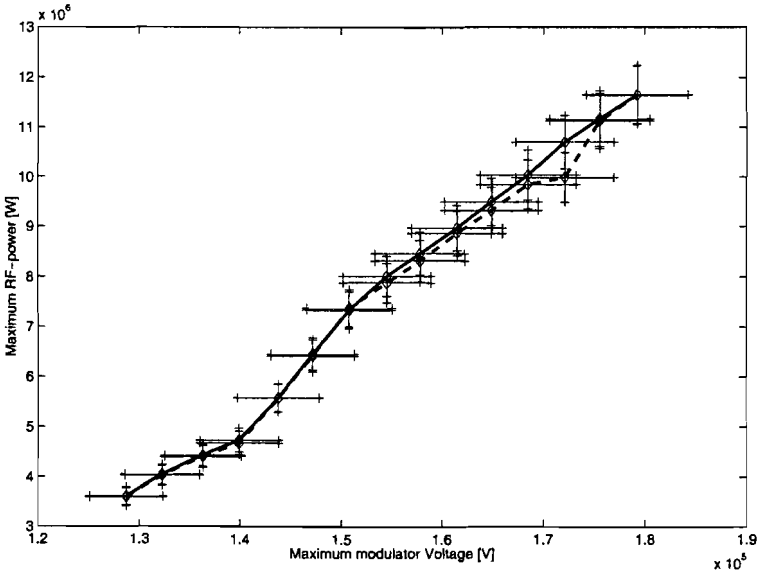

Figure 3.6: Measured klystron output power

Figure 3.6 shows the maximum RF output power as a function of the maximum modulator output voltage. The solid line shows the factory settings and the dotted line shows the settings after changing the current through the first focusing coil. For low modulator voltages the output power stays the same but around $10MW$ the klystron RF output power drops a little due to the mismatch in the focusing current. Since the cavity is used at approximately $5MW$ at the moment the setting using the modified focusing current is used.

When the klystron input voltage is increased further the output RF-power starts to increase again but the shape of the RF-pulse coming out of the klystron becomes very irregular. The exact shape and place of these irregularities are slightly unstable over time which could spoil the overall stability of the system. The simple approximation of a static input-output power relation cannot be used to predict the behavior of these irregularities so it is not recommended to use these settings. Measuring at higher powers is dangerous because the maximum voltage coming out of the modulator then approaches the breakdown voltage of the klystron tube ($U_{breakdown} = 193kV$) which could damage the tube.

There where some uncertainties regarding the measurements of the modulator voltage. The calibration report of the manufacturer of the capacitive divider contained some errors. The correspondence with the manufacturer of the divider did not provide much extra information so a different calibration approach was used to check the measurements. It is possible to determine the input voltage of the klystron tube by using the information provided by the manufacturer. Using this method it is possible to calibrate the system very accurately. Using equation 3.2, and the klystron efficiency $\mu = 0.49$ at $10MW$ RF output power the input voltage can be determined with a worst case accuracy of 2.8%.

$$U_{mod}(t) = K^{-\frac{2}{5}} P_{mod}(t)^{\frac{2}{5}} \tag{3.2}$$

Figure 3.7 shows the modulator output voltage as a function of time using the calibration factor specified by the manufacturer of the high voltage capacitive divider (solid line). The dotted lines give the accuracy of the measurement provided by the manufacturer (5%). Figure 3.7 also shows the maximum voltage calculated using the klystron factory calibration as described above (with an accuracy of 2.8%) which is given by the diamond shaped point.

3.3.2 Klystron phase measurements

The large signal phase measurements of the RF signal coming out of the klystron present a new problem since the phase variations are much larger than π *rad.* Such a large phase variation is impossible to measure accurately using the multiplier phase measurement system shown in figure 2.1 since the output of the system gives the cosine of the phase which cannot be reconstructed accurately over the full range of phase variations. Since the first predictions using the non-relativistic phase model (see section 2.3.1) predicted a very large phase variation the initial approach of the problem included a phase compensation by using feed-forward compensation. After implementation of a feed-forward compensation it might be possible to use this system because then the measurement system will only measure the phase error which should be smaller than π *rad.* Since the influence of phase variation on the acceleration field is less severe, because of the relativistic effect (see section 2.3.2), the phase compensation is not implemented.

In order to measure the large signal phase it is possible to use a frequency divider which not only divides the input frequency ω_0 by a factor N_{div} but also divides the phase information $\phi_{in}(t)$ by a factor N_{div}. The problem with using this technique is that the dividers work by

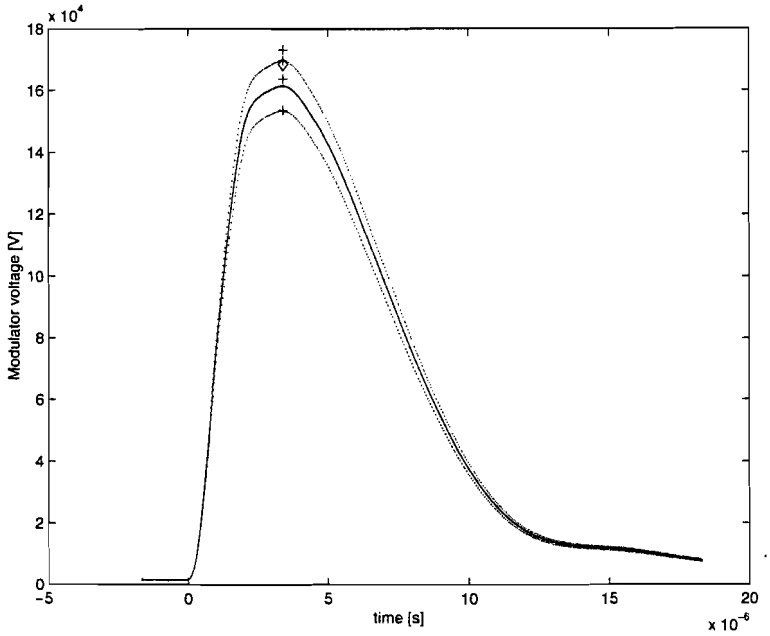

Figure 3.7: Power and voltage measurement verification

counting the zero crossings of the input RF signal. The number of zero crossings is then divided by the division ratio N_{div}.

The division technique described above works fine for continuous wave input signals but the output signal of the klystron is pulsed. There is some jitter between the RF-signal and the timing of the modulator triggering and there is some noise on the output RF signal amplitude of the klystron. Because of the jitter and the noise on the amplitude the zero crossing at which the divider starts counting is random which causes a random phase offset of the divided output signal compared to the input signal. The division ratio N_{div} of the dividers is set to 8 which gives a output frequency of approximately $375MHz$. This means that there are 16 zero crossings of the input signal per output period. After mixing the divided input oscillator signal with the divided klystron RF output signal there are eight random phase offsets and the measured phase difference has two possible random signs per offset. This makes it almost impossible to implement this setup as a sensor for a controller but by rejecting all output signals except for one it is possible to use it to determine the phase of the output signal although the phase offset information is lost.

Since the dividers count zero crossings the bandwidth of the system is limited to a theoretical maximum (using the Nyquist criteria) of $187.5MHz$ which is still large enough to measure the phase variations accurately. Figure 3.8 shows the measured phase (in degrees) as a function of time for increasing modulator voltages. Since the offset is lost the minimum phase is corrected to zero which is of no real importance because the accelerator cavity is only sensitive to phase changes. Figure 3.9 shows the large signal measurement reconstruction of the instantaneous frequency deviation (in [Hz]). This signal is the derivative of the measured phase signal. There are a few strange phenomena visible in the frequency deviation plot. The frequency deviation shows a few strange irregularities which can be correlated to the irregularities in the RF output power of the klystron. These irregularities are not present in the simulated output phase. The irregularities are probably caused by space charge effects

and large modulation indexes which are not accounted for in the simulation model. The simulation model is validated by inserting the measured modulator voltage as discussed in section 3.2. The simulated version of the instantaneous frequency deviation is shown in figure 3.10. The small oscillation which is present in both the simulation and the measurement is due to oscillations caused by resonant modes of the pulse transformer which are not completely damped.

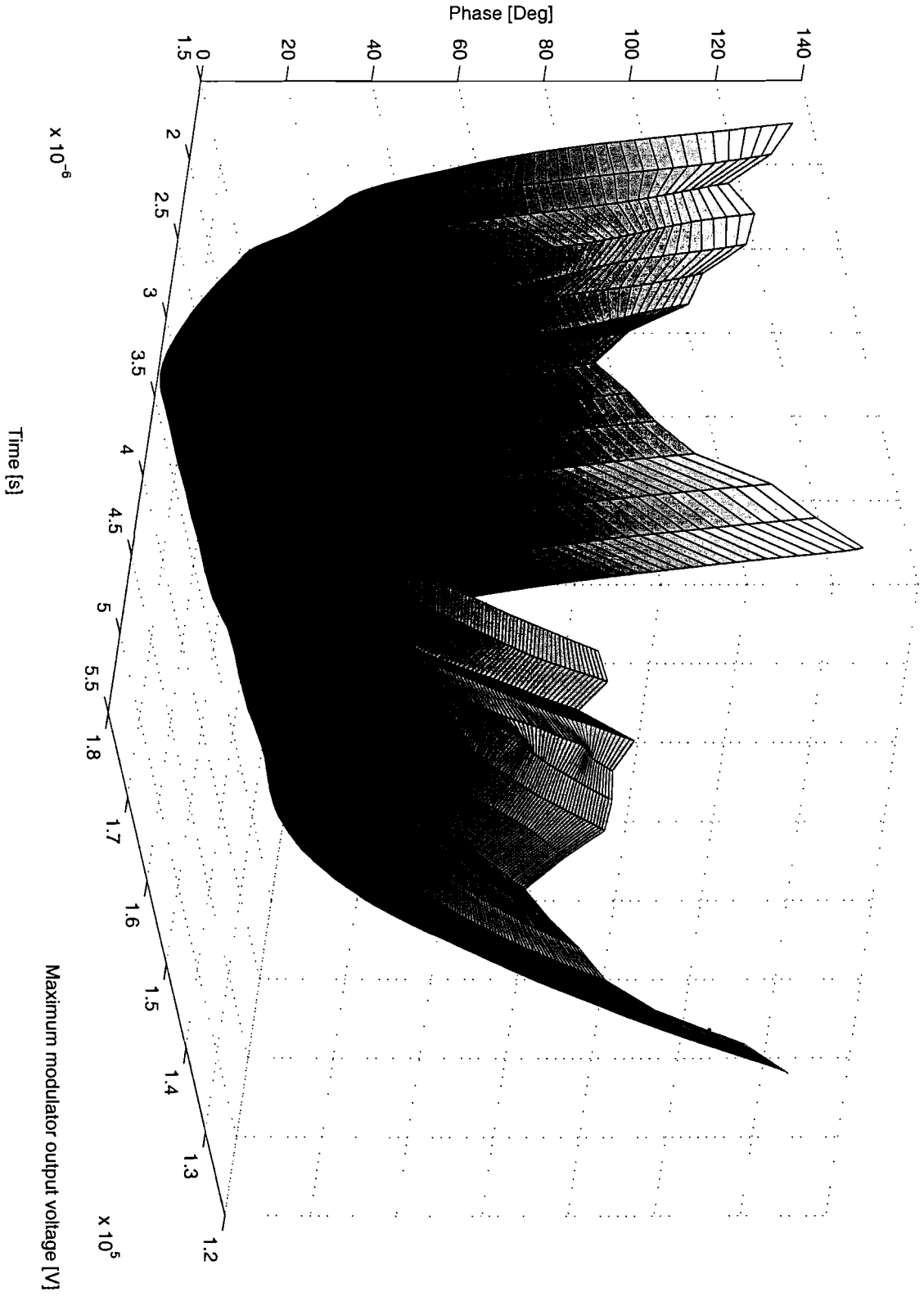

Figure 3.8: Phase as a function of time for increasing maximum modulator voltage

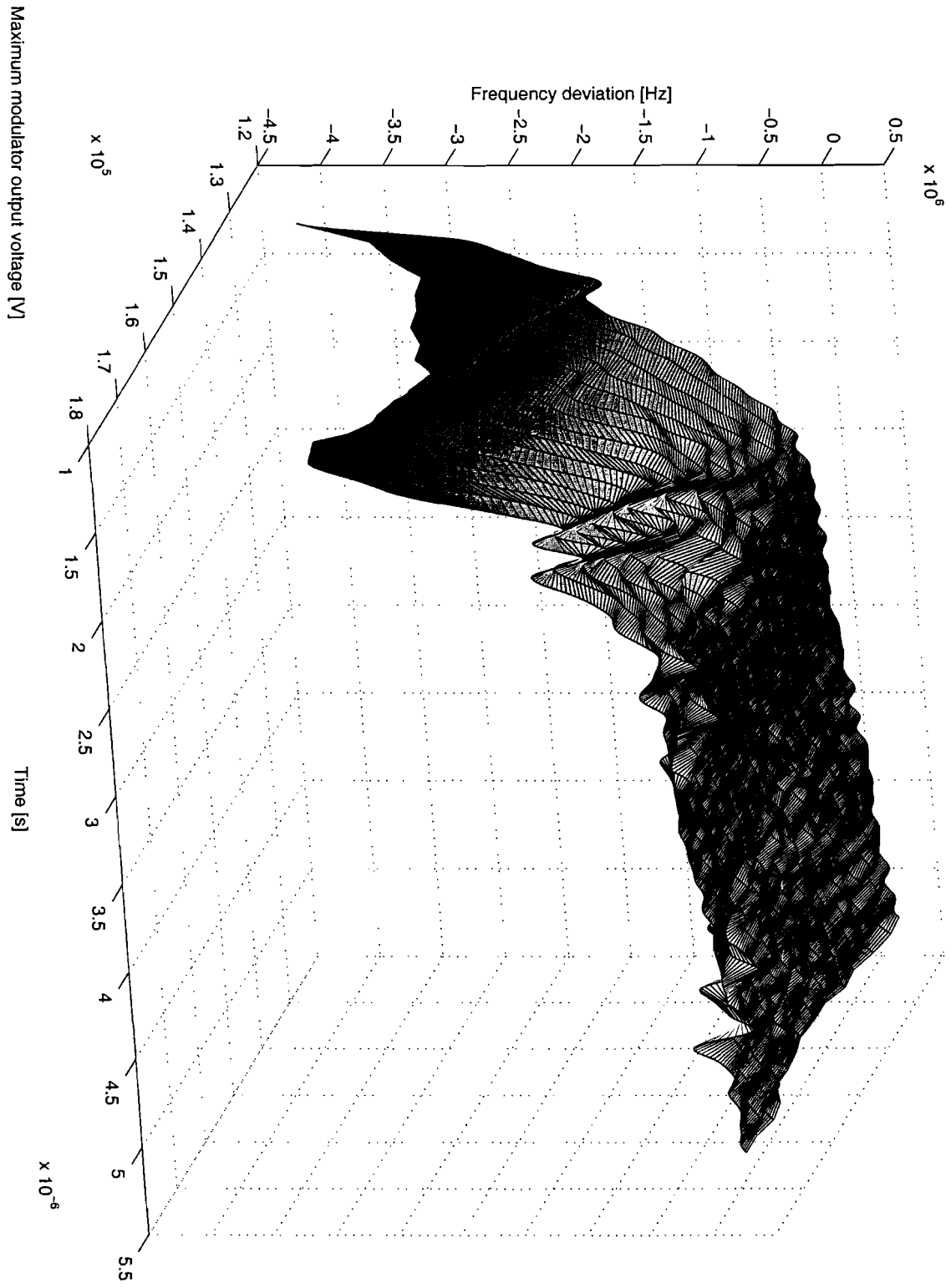

Figure 3.9: Measured instantaneous frequency deviation for increasing maximum modulator voltage

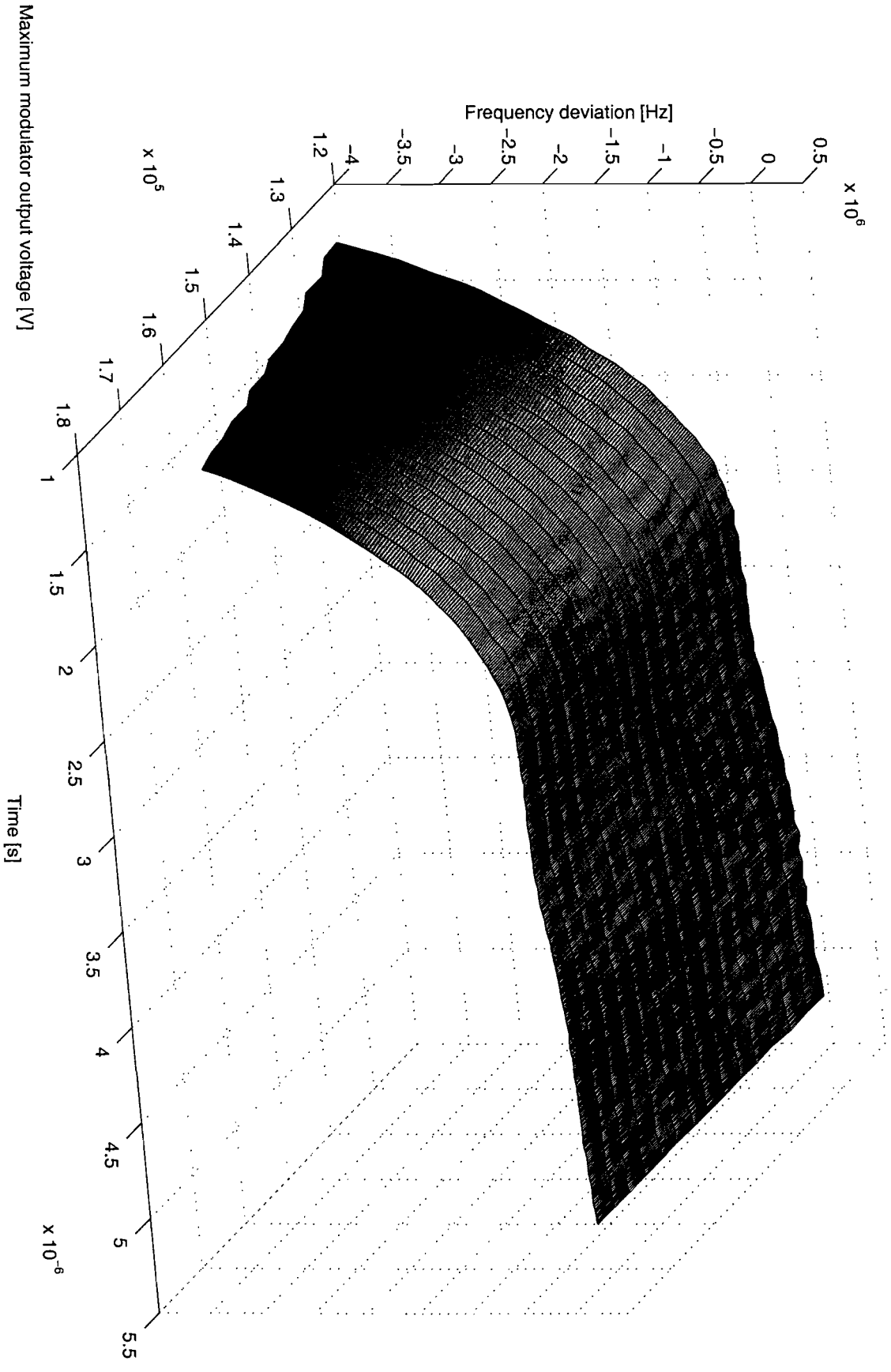

Figure 3.10: Simulated instantaneous frequency deviation for increasing maximum modulator voltage

3.4 Cavity measurements

Since the cavity is connected to the klystron tube by a waveguide with two directional couplers it is possible to measure the forward RF-power, from the klystron tube towards the accelerator cavity, and the power reflected by the cavity. In steady state at resonance using a optimal matching, the reflected power should be zero. Because of the instantaneous frequency deviation and because of the limited bandwidth of the cavity some of the power will be reflected. The power absorbed by the cavity is given by:

$$P_{transmitted}(t) = \frac{dW_{tot}(t)}{dt} + \frac{\omega_0 W_{tot}(t)}{Q} \tag{3.3}$$

where W_{tot} is the total average energy stored in the cavity and $\frac{\omega_0 W_{tot}(t)}{Q}$ is the rate of dissipation of energy into the losses in the cavity. Figure 3.11 shows a typical measurement at a peak RF-power of approximately $4MW$. The solid line shows $P_{forward}$ and the dashed line shows $P_{reflected}$. A more detailed description of the cavity is given in section 2.4 and in chapter 4.

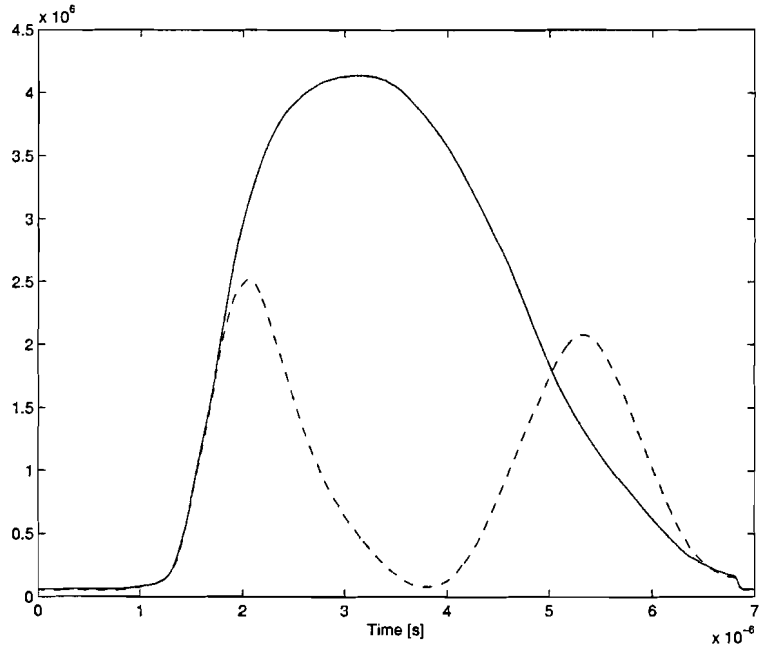

Figure 3.11: Typical cavity behavior at low power

Chapter 4

Simulation and analysis results

4.1 Introduction

In this chapter the problems presented in the problem definition (section 1.2) are analyzed using the models derived in chapter 2 and the measurements of chapter 3. It is possible to simulate the cavity behavior by using the lumped circuit equivalent described in section 2.4. First section 4.2 shows the analytic solution of the step-response of the cavity energy on an RF power step with a constant RF phase. Section 4.2 is included to show the ideal cavity behavior when using a flat-top modulator pulse. Section 4.3 shows the influence of using an "exponentially shaped" modulator pulse on the cavity behavior by comparing it to the ideal situation presented in section 4.2. Finally section 4.4 shows the influence of the "exponentially shaped" pulse on the phase jitter.

4.2 The analytical solutions of the cavity behavior.

It is possible to derive an analytical solution describing the step-response at resonance, on an RF power step, of the total average stored cavity energy. This is done using the lumped circuit equivalent described in section 2.4. The step-response shows the behavior of the accelerator cavity when using an ideal flat-top modulator pulse.

This section describes the derivation of this step-response. The total stored energy is the sum of the electric energy and the magnetic energy as shown by equation 4.1.

$$W_{st}(t) = W_e(t) + W_m(t) \tag{4.1}$$

At resonance $\omega = \omega_0\sqrt{1 - \frac{1}{4Q_l^2}} \approx \omega_0$ the average stored electric energy equals the average stored magnetic energy resulting in equation 4.2.

$$\langle W_{st}(t)\rangle_T = 2\langle W_e(t)\rangle_T = 2\langle W_m(t)\rangle_T \tag{4.2}$$

When using a lumped network equivalent the voltage across the capacitor is proportional with the electric field inside the cavity and the current through the inductance is proportional with the magnetic field inside the cavity. Using this the electric energy translates into the energy stored in the capacitance and the magnetic energy translates into the energy stored in the inductance (equations 4.3 and 4.4).

$$\langle W_C(t)\rangle_T = \frac{1}{4}C\,|\hat{u}_c(t)|^2 \tag{4.3}$$

$$\langle W_L(t)\rangle_T = \frac{1}{4}L\left|\hat{i}_L(t)\right|^2 \tag{4.4}$$

The klystron always delivers power into a matched load (by using a circulator). This means that the total dissipated power of the klystron P_{tot} is dissipated into R_l. When assuming a matched load the total dissipated power is twice the power delivered to the cavity resistance R (which is explained in section 2.4). By using this relation it is possible to calculate the total current amplitude $\hat{i}_k$ as shown in equation 4.5.

$$\hat{i}_k(t) = \sqrt{\frac{2P_{tot}}{R_l}}\varepsilon(t) \tag{4.5}$$

Appendix F shows the derivation of the step-response of the total stored average energy at resonance using a matched load (by using the complex envelope baseband transformation) which is given by:

$$\langle W_{st}(t)\rangle_T = P_{tot}\frac{Q_l}{\omega_0}\left\{1 - e^{-\frac{\omega_0}{2Q_l}t}\right\}^2 \tag{4.6}$$

Figure 4.1 shows the total stored average energy (the dotted line shows the steady state value). Figure 4.2 shows the normalized electric field amplitude, which equals the normalized

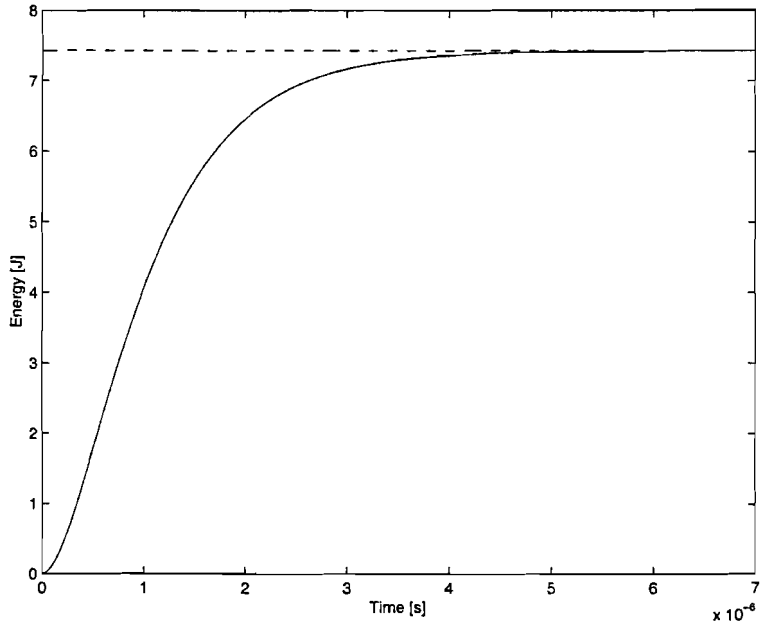

Figure 4.1: Total stored average energy.

voltage amplitude across the capacitor, as a function of time.

4.3 Phase and amplitude variation influence.

In this section the influence of large phase variations and amplitude variations on the cavity behavior will be discussed. Section 4.2 is meant as an introduction to this section since it shows the cavity behavior using a flat top modulator pulse without any phase variations. This section compares the simulations using an "exponentially shaped" modulator pulse with the

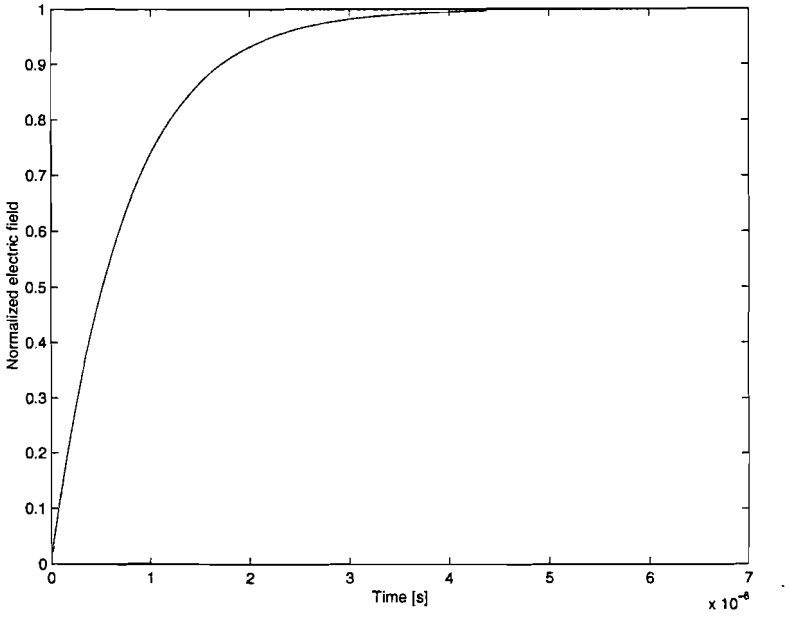

Figure 4.2: Normalized electric field amplitude.

ideal situation calculated in section 4.2. This section also uses the complex envelope models derived in sections E.1 and E.2. A short explanation of the models and of the complex envelope transformation can be found in section 2.4 of this document.

When using the lumped circuit equivalent of the cavity the total average stored energy equals:

$$\langle W_{st}(t)\rangle_T = \langle W_C(t)\rangle_T + \langle W_L(t)\rangle_T = \frac{1}{4}C\left|\hat{u}_c(t)\right|^2 + \frac{1}{4}L\left|\hat{i}_L(t)\right|^2 \tag{4.7}$$

Since the cavity is excited off resonance by a non-linear phase and amplitude function the electric field (proportional with the voltage across the capacitance), and the magnetic field (proportional with the current through the inductance) must be solved numerically. In order to do this the inductance current RF amplitude $\hat{i}_L(t)$ and the capacitance voltage amplitude $\hat{u}_c(t)$ must be calculated by using the complex envelope description described in section 2.4.

$$g_{i_k}(t) = \hat{i}_k(t)e^{j\phi(t)} \tag{4.8}$$

$$\frac{1}{2}g_{i_L}(t) = \frac{1}{2}g_{i_k}(t) * \frac{1}{2}k_{h_i}(t) \tag{4.9}$$

$$\hat{i}_l(t) = \left|g_{i_L}(t)\right| \tag{4.10}$$

$$\frac{1}{2}g_{u_C}(t) = \frac{1}{2}g_{u_C}(t) * \frac{1}{2}k_Z(t) \tag{4.11}$$

$$\hat{u}_c(t) = \left|g_{u_C}(t)\right| \tag{4.12}$$

Equations 4.8 to 4.12 show the proper convolution of the input signals, transformed to a baseband equivalent g (this is done by eliminating ω_0 using the complex envelope representation), with the baseband equivalent of the cavity impulse response k. The reason for choosing lower case variable names is explained in section 2.4.2. Because the complex envelope function describes the RF output amplitude at resonance, and the phase changes per RF period are

assumed very small, the average electric energy and the average magnetic energy contribution per RF period are also equal to each other when the cavity is excited off resonance. Using the equality it is possible to simulate the total stored average energy using only the voltage across the capacitance (the simulation error and the numerical simulation accuracy is in the same order of magnitude). The changing phase influence on the RF phase of the electric field inside the cavity can also be calculated using the complex envelope method:

$$\phi_{E_{cav}}(t) = \angle g_{u_C}(t) = \arctan\left(\frac{im(g_{u_C}(t))}{re(g_{u_C}(t))}\right) \tag{4.13}$$

Using equations 4.8 to 4.13 it is now possible to simulate the stored average cavity energy. First this is done by using the simulated phase and power coming out of the klystron at nominal input power. The output RF power as a function of the input RF power is calculated by using the efficiency of 49% at $10MW$ given by the manufacturer of the klystron tube and the 5% loss of the circulator. This is not very accurate but it does show the effect of an "exponentially shaped" RF power pulse on the behavior of the cavity without all the non-linear effects of the klystron power.

The solid line in figure 4.3 shows the average stored cavity energy as a function of time when using a simulated "exponentially shaped" klystron output RF power (with a peak RF output-power of $10MW$) when including the effect of the simulated phase change. The dashed line shows the average stored energy going into the cavity using the same power pulse but without the phase changes (which is the maximum achievable energy using ideal phase compensation). The dash-dotted line shows the analytic result when using an ideal flat modulator pulse.

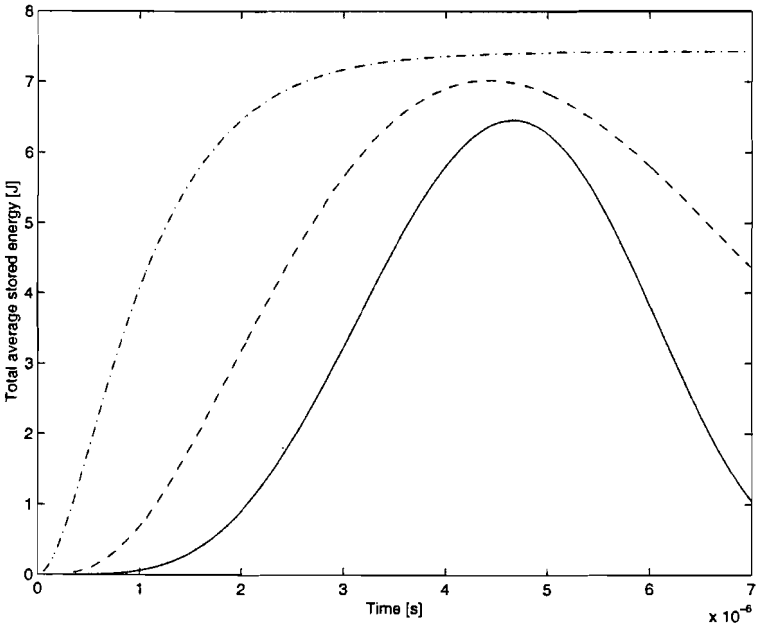

Figure 4.3: Total stored average energy as a function of time.

Figure 4.4 shows the simulated percentage of average electric RF field decrease relative to the maximum attainable steady state electric field inside the cavity. The solid line shows the influence of the phase variations on the output power. The dashed line shows the influence

on the electric field because of the fact that the cavity is unable to reach its final steady state value due to its high loaded quality factor Q_l. And finally the dash-dotted line shows the total loss of electric field due to the combination of both effects.

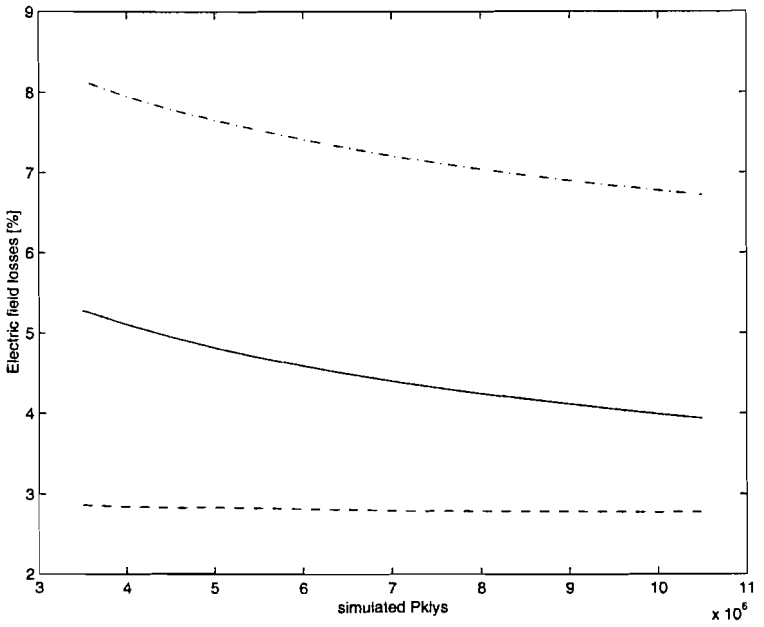

Figure 4.4: Simulated perc. of electric field losses as a function of klystron RF power.

Since the klystron RF output power as a function of the input power is a non-linear function and the phase contains several irregularities the simulations presented above are repeated using the measured klystron phase and output RF power.

Figure 4.5 shows the average stored energy going into the cavity. The solid line in figure 4.5 shows the average stored cavity energy as a function of time when using the measured "exponentially shaped" klystron output RF power (with a peak RF output-power of $10MW$) when including the effect of the measured phase change. The value of the klystron RF output power is 5% larger because the circulator causes a power loss of 5%. The dashed line shows the average stored energy going into the cavity using the same power pulse but without phase changes (which is the maximum achievable energy using ideal phase compensation). The dash-dotted line shows the analytic result when using an ideal flat modulator pulse (with the same maximum klystron RF output power of $10MW$). The decrease of the maximum stored average energy due to phase changes using a klystron peak RF output-power of $10MW$ (solid line) compared to the situation using ideal compensation (dashed line) is approximately 10%. The maximum attainable increase in energy when using a wider input pulse (enabling the cavity to approach steady state conditions) is equal to approximately 10%. This results in a total loss of energy equal to 20%. Since the energy is proportional with the square of the electric field, the influence of the phase changes on the acceleration field is equal to approximately half the percentages given for the average stored energy. Figure 4.6 shows the percentage of average electric RF field decrease relative to the maximum attainable steady state electric field inside the cavity. The solid line shows the influence of the phase variations on the maximum electric field. The dashed line shows the influence on the maximum electric field caused by the limited bandwidth of the cavity due to its high loaded quality factor Q_l.

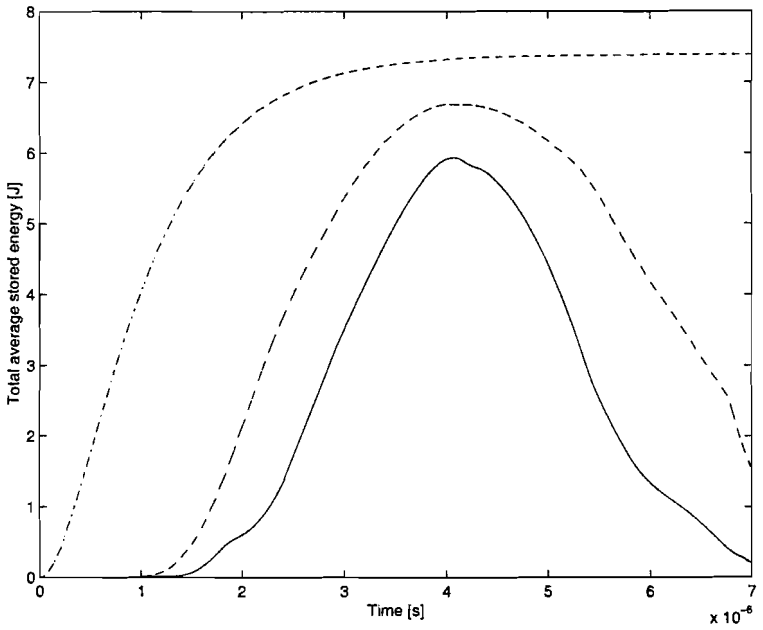

Figure 4.5: Total stored average energy as a function of time.

And finally the dash-dotted line shows the total loss of electric field due to the combination of both effects. The energy deficit (of the simulation using measured data), caused by a

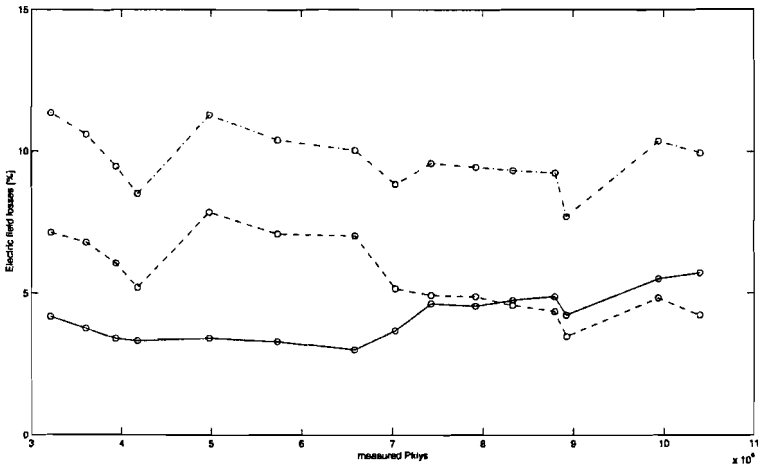

Figure 4.6: Percentage of electric field losses as a function of klystron RF power.

too short filling time of the cavity, is approximately twice as high as the simulated energy loss (using all the models and a linear klystron input-output relation) and it contains some irregularities (dashed line). This is caused by the non-linear input power to output power relation of the klystron. The efficiency at low RF output power of the klystron is very low which results in a shorter pulse. This shorter pulse prevents the cavity from reaching its steady state value, resulting in a larger error. The irregularities are caused by the changing

klystron power sensitivity S given by:

$$S = \frac{dP_{out}(P_{in})}{dP_{in}} \tag{4.14}$$

When the sensitivity around maximum output power is very low the output pulse becomes flat in that region resulting in a larger end value of the cavity energy and thus in a smaller energy loss. The energy loss caused by phase changes during the pulse is actually somewhat smaller because of the low klystron efficiency at low power which decreases the effect of large phase changes at low power and because of the flat parts in the modulator voltage pulse (shown in section 3.2). The increase of the losses (compared to the simulation model) at high power is caused by the irregularities on the measured frequency deviation (which is not included in the model as can be seen from figures 3.9 and 3.10) which slowly become dominant at higher powers of the measured data simulation.

4.4 Phase stability analysis.

This section contains some information about the phase jitter caused by various components in the system. The synchronization of the laser pulses to the RF signal has a standard deviation of $\sigma_{t_{sync}} = 20fs$ or $\sigma_{\phi_{sync}} = 0.38 \cdot 10^{-3} rad$.

When using a flat top modulator pulse, the pulse to pulse phase stability of the phase coming out of a klystron, which is equal to the pulse to pulse phase stability of the phase inside the cavity, is mainly determined by the pulse to pulse stability of the modulator voltage pulse. It is possible to derive an equation describing the phase stability $d\phi$ as a function of the fractional voltage fluctuations:

$$d\phi = -\frac{\omega_0 d_2}{c} \frac{1}{(\gamma+1)\sqrt{\gamma^2-1}} \frac{dU_{mod}}{U_{mod}} \tag{4.15}$$

When using an "exponentially shaped" modulator pulse the analysis become slightly more complex. Equation 4.15 can still be used but the phase of the RF field inside the cavity is not constant during the pulse.

The phase noise resulting from the voltage stability of the high voltage source of the modulator (measured: 0.05%) at nominal operation ($U_{mod} = 169kV$) equals:

$$\sigma_{\phi_{volt}} \approx 11.7 \frac{\sigma_{U_{mod}}}{u_{mod}} \approx 5.8 \cdot 10^{-3} rad \tag{4.16}$$

This phase stability has also been measured by mixing the input and output RF signal of the klystron. The measured standard deviation equals $6 \cdot 10^{-3} rad$. At maximum RF field the RF frequency inside the cavity is slightly off resonance ω_{cavdet}. The phase stability from pulse to pulse has become sensitive to time jitter dt_{sync} between the modulator trigger pulse and the laser pulse. The time jitter has a standard deviation $\sigma_{t_{mod}}$ of approximately $10ns$. The phase jitter as a result of this time jitter is equal to:

$$d\phi_{time} = \omega_{cavdet}|_{E_{maxRF}} dt_{sync} \tag{4.17}$$

At nominal operation ($10MW$ klystron RF power) the ω_{cavdet} component is approximately $4.5 \cdot 10^5 rad/s$. The standard deviation of the phase jitter $\sigma_{\phi_{time}}$ as a result of the time jitter

at nominal operation is equal to approximately $4.5 \cdot 10^{-3} rad$. When assuming that all noise components are uncorrelated and assuming a white Gaussian noise distribution the standard deviation of the total phase noise at nominal operation can be calculated by:

$$\sigma_{\phi_{tot}} = \sqrt{(\sigma_{\phi_{time}})^2 + (\sigma_{\phi_{volt}})^2 + (\sigma_{\phi_{sync}})^2} \tag{4.18}$$

This results in a standard deviation of the total phase jitter of $7.4 \cdot 10^{-3} rad$. The total phase jitter can be converted to a time jitter by using the resonant frequency (ω_0):

$$\sigma_{t_{tot}} = \frac{\sigma_{\phi_{time}}}{\omega_0} \tag{4.19}$$

The calculated standard deviation of the total time jitter of the system equals $3.9 \cdot 10^2 fs$. When a flat modulator pulse is used the total time jitter would be $3.1 \cdot 10^2 fs$ which is approximately 25% smaller.

Chapter 5

Conclusions and recommendations

5.1 Problem definition

Usually the modulator is designed to deliver a flat top power pulse. This is done by using a pulse forming network, containing a lot of high voltage capacitors and inductors, which simulates a long line. In the setup which is built at Eindhoven University of Technology a different approach is used. Instead of using a modulator creating a flat top pulse the modulator was designed to create an "exponentially shaped" pulse. The reasons for choosing an "exponentially shaped" pulse instead of a flat top pulse are:

- only one short electron bunch is accelerated per RF power pulse (which consumes only a very small fraction of the power) so there is no need for a constant output power.
- the modulator becomes very compact because it contains less large high voltage and high power components.
- the modulator becomes more reliable mainly because it contains less capacitors.
- the modulator becomes cheaper.

However there are problems connected with using an "exponentially shaped" pulse to power the klystron tube. Firstly the tube introduces a frequency change. This is caused by the changing acceleration voltages in the klystron which causes the output frequency of the klystron tube to shift with respect to its input frequency. Since the RF accelerator cavity has an extremely small bandwidth the changing delay causes the cavity to be shifted off resonance which means that the maximum RF field in the cavity will be smaller.

The second problem is that because of the changing frequency the phase of the RF field inside of the cavity will have a small time-dependency which could increase the phase jitter between the laser and the RF field inside the cavity. This might spoil the stability of the accelerator.

The third problem is caused by the shape of the pulse itself. Since the cavity has a very high quality factor it has a limited bandwidth which prevents it from reaching its maximum (steady state) value. This also results in a decrease of the maximum RF field inside the cavity.

5.2 Conclusions

The disadvantages, which are explained in the problem definition, where analyzed in this document (mainly in chapter 4). This section contains the results.

The overall decrease of the electric RF field inside the cavity when using an "exponentially shaped" modulator pulse, equals approximately 10% of which approximately 5% is caused by the klystron output frequency change (see figure 4.6). The 5% loss of electric field due to phase changes is actually much less than the initial guess. There is one main reasons why the phase influence is much less than initially expected. The phase changes are caused by changes of the beam velocity inside the klystron. The relativistic effect reduces the phase variations around maximum because it can be seen as a saturation effect (see section 2.3). Another reason why the phase variations are less severe is the flat straight slope around the maximum of the modulator output pulse at the secondary side of the pulse transformer which slightly reduces the phase variation around maximum.

The phase jitter is slightly larger when using an "exponentially shaped" modulator pulse instead of a flat modulator pulse. The total time jitter resulting from the phase jitter has a standard deviation of approximately $3.9 \cdot 10^{-13}s$. When using a flat top pulse the standard deviation of the total jitter could have been approximately 25% smaller (see section 4.4).

The phase variations introduced by the klystron can be compensated using a phase shifter but this would require a combination of a very accurate feed-forward and feedback phase compensation over a large output range which would improve the maximum energy in the cavity with less than 5%. Since the improvement of implementing such a system is very small and because of the difficulties of implementing a feed-forward and feed-back system it is not advisable to build such a controller. The total phase-jitter can be reduced by approximately 25% when using only feed-forward compensation to reduce the phase variation at maximum electric field inside the cavity, which reduces the phase jitter caused by the synchronization jitter between the modulator and the RF-signal phase. A larger reduction can be obtained by improving the stability of the power source.

5.3 Recommendations

The total process has been analyzed and the improvement of the system by implementing a phase compensation controller is actually very small. In order to improve the phase jitter of the system it might still be interesting to implement a phase compensation controller but the jitter is already small enough for most applications of the accelerator. There still is one phenomenon that is interesting for further study which is the straight part in the modulator pulse around maximum (see section 3.2) because it would increase the accuracy of the model and it causes a constant frequency de-tuning which can easily be compensated for by de-tuning the input frequency. This would create a feed-forward compensation which increases the maximum electric field inside the cavity without having to add any extra components to the system.

Appendix A

The non-relativistic deviation frequency derivation

$$d\phi(t) = -\frac{d_2\omega_0}{v_e^2(t)}dv_e(t) \tag{A.1}$$

$$W_k = \frac{1}{2}m_0 v_e^2(t) \tag{A.2}$$

$$W_p = qU_{mod}(t) \tag{A.3}$$

$$v_e(t) = \sqrt{\frac{2qU_{mod}(t)}{m_0}} \tag{A.4}$$

$$dv_e(t) = \frac{2\frac{q}{m_0}}{2\sqrt{\frac{2qU_{mod}(t)}{m_0}}}dU_{mod}(t) = \frac{v_e(t)}{2U_{mod}(t)}dU_{mod}(t) \tag{A.5}$$

$$\frac{dv_e(t)}{v_e(t)} = \frac{1}{2}\frac{dU_{mod}(t)}{U_{mod}(t)} \tag{A.6}$$

$$\omega_{\text{det}}(t) = \frac{d\phi(t)}{dt} = -\frac{\omega_0 \cdot d_2}{2\sqrt{\frac{2q}{m_0}}U_{mod}^{3/2}(t)}\frac{dU_{mod}(t)}{dt} \tag{A.7}$$

$$\omega_{det}(t) = -\frac{\omega_0 d_2}{v_e(t)}\frac{1}{U_{mod}(t)}\frac{1}{2}\frac{dU_{mod}(t)}{dt} \tag{A.8}$$

Appendix B

The non-relativistic transition-time derivation

$$E(t, t_z) = \frac{U_{mod}(t + t_z)}{d_1} \tag{B.1}$$

$$F(t, t_z) = qE(t, t_z) \tag{B.2}$$

$$\underset{t_0 \in \mathbb{R}}{\forall} m_0 a_{ze}(t = t_0, t_z) = F(t = t_0, t_z) \tag{B.3}$$

$$z(t, t_z = 0) = 0 \tag{B.4}$$

$$v_{ze}(t, t_z = 0) = 0 \tag{B.5}$$

$$\underset{t_0 \in \mathbb{R}}{\forall} a_{ze}(t = t_0, t_z) = \frac{qU_{mod}(t_0 + t_z)}{d_1 m_0} \tag{B.6}$$

$$\underset{t_0 \in \mathbb{R}}{\forall} \frac{dv_{ze}(t = t_0, t_z)}{dt_z} = a_{ze}(t = t_0, t_z) \tag{B.7}$$

$$\underset{t_0 \in \mathbb{R}}{\forall} \frac{dz(t = t_0, t_z)}{dt_z} = v_{ze}(t = t_0, t_z) \tag{B.8}$$

$$t_{tr}(t) = (t_z | z(t - t_z, t_z) = d_1) \tag{B.9}$$

$$v_e(t) = v_{ze}(t - t_{tr}(t), t_{tr}(t)) \tag{B.10}$$

$$d\phi(t) = -\frac{d_2 \omega_0}{v_e^2(t)} dv_e(t) \tag{B.11}$$

$$\omega_{det}(t) = \frac{d\phi(t)}{dt} = -\frac{d_2 \omega_0}{v_e^2(t)} \frac{dv_e(t)}{dt} \tag{B.12}$$

Appendix C

The relativistic deviation frequency derivation

$$W_k(t) = \left(\frac{1}{\sqrt{1 - \frac{v_e^2(t)}{c^2}}} - 1 \right) m_0 c^2 \tag{C.1}$$

$$W_p(t) = eU \tag{C.2}$$

$$\gamma = \frac{eU}{m_0 c^2} + 1 \tag{C.3}$$

$$\frac{v_e^2(t)}{c^2} = 1 - \frac{1}{\gamma^2} \tag{C.4}$$

$$v_e(t) = c\sqrt{1 - \frac{1}{\gamma^2}} \tag{C.5}$$

$$d\gamma(t) = \frac{e}{m_0 c^2} dU_{mod}(t) = (\gamma(t) - 1) \frac{dU_{mod}(t)}{U_{mod}(t)} \tag{C.6}$$

$$d\phi(t) = -\frac{d_2 \omega_0}{c} \frac{\gamma(t) - 1}{(\gamma^2(t) - 1)^{\frac{3}{2}}} \frac{dU_{mod}(t)}{U_{mod}(t)} = -\frac{d_2 \omega_0}{c} \frac{1}{(\gamma(t) + 1)\sqrt{\gamma^2(t) - 1}} \frac{dU_{mod}(t)}{U_{mod}(t)} \tag{C.7}$$

$$\omega_{det}(t) = \frac{d\phi(t)}{dt} = -\frac{d_2 \omega_0}{c} \frac{1}{(\gamma(t) + 1)\sqrt{\gamma^2(t) - 1}} \frac{1}{U_{mod}(t)} \frac{dU_{mod}(t)}{dt} \tag{C.8}$$

$$\omega_{det}(t) = -\frac{d_2 \omega_0}{v_e(t)} \frac{1}{\gamma(t)(\gamma(t) + 1)} \frac{1}{U_{mod}(t)} \frac{dU_{mod}(t)}{dt} \tag{C.9}$$

Appendix D

The relativistic transition-time derivation

$$E(t,t_z) = \frac{U_{mod}(t+t_z)}{d_1} \tag{D.1}$$

$$F(t,t_z) = qE(t,t_z) \tag{D.2}$$

$$\underset{t_0\in\mathbb{R}}{\forall} F(t=t_0,t_z) = \frac{dp_{ze}(t=t_0,t_z)}{dt_z} = \frac{d}{dt_z}\left(\frac{m_0 v_{ze}(t=t_0,t_z)}{\sqrt{1-\frac{v_{ze}^2(t=t_0,t_z)}{c^2}}}\right) \tag{D.3}$$

$$\beta(t,t_z) = \frac{v_{ze}(t,t_z)}{c} \tag{D.4}$$

$$\underset{t_0\in\mathbb{R}}{\forall} F(t=t_0,t_z) = \frac{d}{dt_z}\left(m_0 c\frac{\beta(t=t_0,t_z)}{\sqrt{1-\beta^2(t=t_0,t_z)}}\right) \tag{D.5}$$

$$\underset{t_0\in\mathbb{R}}{\forall} F(t=t_0,t_z) = m_0 c\left(\frac{1}{\sqrt{1-\beta^2(t=t_0,t_z)}} + \frac{\beta^2(t=t_0,t_z)}{(1-\beta^2(t=t_0,t_z))^{\frac{3}{2}}}\right)\frac{d\beta(t=t_0,t_z)}{dt_z} \tag{D.6}$$

$$\underset{t_0\in\mathbb{R}}{\forall} F(t=t_0,t_z) = m_0 c\frac{1}{(1-\beta^2(t=t_0,t_z))^{\frac{3}{2}}}\frac{d\beta(t=t_0,t_z)}{dt_z} \tag{D.7}$$

$$\underset{t_0\in\mathbb{R}}{\forall} \frac{d\beta(t=t_0,t_z)}{dt_z} = \frac{F(t=t_0,t_z)}{m_0 c}\left(1-\beta^2(t=t_0,t_z)\right)^{\frac{3}{2}} \tag{D.8}$$

$$z(t,t_z=0) = 0 \tag{D.9}$$

$$\beta(t,t_z=0) = 0 \tag{D.10}$$

$$\underset{t_0\in\mathbb{R}}{\forall} \frac{d\beta(t=t_0,t_z)}{dt_z} = \frac{q}{d_1 m_0 c}U_{mod}(t_0+t_z)\left(1-\beta^2(t=t_0,t_z)\right)^{\frac{3}{2}} \tag{D.11}$$

$$\underset{t_0 \in \mathbb{R}}{\forall} \frac{dz(t = t_0, t_z)}{dt_z} = c\beta(t = t_0, t_z) \tag{D.12}$$

$$v_{ze}(t, t_z) = c\beta(t, t_z) \tag{D.13}$$

$$t_{tr}(t) = (t_z | z(t - t_z, t_z) = d_1) \tag{D.14}$$

$$v_e(t) = v_{ze}(t - t_{tr}(t), t_{tr}(t)) \tag{D.15}$$

$$d\phi(t) = -\frac{d_2\omega_0}{v_e^2(t)} dv_e(t) \tag{D.16}$$

$$\omega_{det}(t) = \frac{d\phi(t)}{dt} = -\frac{d_2\omega_0}{v_e^2(t)} \frac{dv_e(t)}{dt} \tag{D.17}$$

Appendix E

A complex low-pass equivalent of the cavity

E.1 derivation of the impedance baseband transform

$$Z_l(\omega) = \frac{\frac{R_l}{Q_l}}{\frac{1}{Q_l} + j\left(\frac{\omega}{\omega_0} - \frac{\omega_0}{\omega}\right)} \tag{E.1}$$

$$Z_l(j\omega) = \frac{\frac{R_l\omega_0}{Q_l} j\omega}{(j\omega)^2 + \frac{\omega_0}{Q_l} j\omega + \omega_0^2} \tag{E.2}$$

Switch to laplace by substituting: $s = j\omega$

$$Z_l(s) = \frac{\frac{R_l\omega_0}{Q_l} s}{s^2 + \frac{\omega_0}{Q_l} s + \omega_0^2} = \frac{\frac{R_l\omega_0}{Q_l} s}{\left(s + \frac{\omega_0}{2Q_l}\right)^2 + \omega_0^2\left(1 - \frac{1}{4Q_l^2}\right)} \tag{E.3}$$

$$Z_l(s) = \frac{R_l\omega_0}{Q_l} \frac{s + \frac{\omega_0}{2Q_l}}{\left(s + \frac{\omega_0}{2Q_l}\right)^2 + \omega_0^2\left(1 - \frac{1}{4Q_l^2}\right)} - \frac{R_l\omega_0}{Q_l} \frac{\frac{\omega_0}{2Q_l}}{\omega_0\sqrt{1 - \frac{1}{4Q_l^2}}} \frac{\omega_0\sqrt{1 - \frac{1}{4Q_l^2}}}{\left(s + \frac{\omega_0}{2Q_l}\right)^2 + \omega_0^2\left(1 - \frac{1}{4Q_l^2}\right)} \tag{E.4}$$

$$z_l(t) = \mathcal{L}^{-1}\{Z_l(s)\} \tag{E.5}$$

$$\begin{aligned} z_l(t) = {} & \frac{R_l\omega_0}{Q_l} \cos\left(\omega_0\sqrt{1 - \frac{1}{4Q_l^2}}t\right) e^{-\frac{\omega_0}{2Q_l}t}\varepsilon(t) \\ & - \frac{R_l\omega_0}{Q_l} \frac{1}{2Q_l\sqrt{1 - \frac{1}{4Q_l^2}}} \sin\left(\omega_0\sqrt{1 - \frac{1}{4Q_l^2}}t\right) e^{-\frac{\omega_0}{2Q_l}t}\varepsilon(t) \end{aligned} \tag{E.6}$$

$$z_l(t) = x_z(t)\cos\left(\omega_0\sqrt{1 - \frac{1}{4Q_l^2}}t\right) - y_z(t)\sin\left(\omega_0\sqrt{1 - \frac{1}{4Q_l^2}}t\right) \tag{E.7}$$

$$z_l(t) = \Re\left(g_z(t)e^{j\omega_0\sqrt{1-\frac{1}{4Q_l^2}}t}\right) \tag{E.8}$$

$$k_z(t) = x_z(t) + jy_z(t) = \frac{R_l\omega_0}{Q_l}(1 + j\frac{1}{2Q_l\sqrt{1-\frac{1}{4Q_l^2}}})e^{-\frac{\omega_0}{2Q_l}t}\varepsilon(t) \tag{E.9}$$

$$K_Z(j\omega) = \mathcal{F}\{k_z(t)\} \tag{E.10}$$

$$K_Z(j\omega) = \frac{R_l\omega_0}{Q_l}\left\{\frac{1 + j\frac{1}{2Q_l\sqrt{1-\frac{1}{4Q_l^2}}}}{j\omega + \frac{\omega_0}{2Q_l}}\right\} \tag{E.11}$$

$$Z_l(\omega) = \frac{1}{2}K_Z\left(\omega - \omega_0\sqrt{1-\frac{1}{4Q_l^2}}\right) + \frac{1}{2}K_Z^*\left(-\omega - \omega_0\sqrt{1-\frac{1}{4Q_l^2}}\right) \tag{E.12}$$

E.2 derivation of the inductance-current baseband transform

$$H_I(s) = \frac{I_L}{I_k}(s) = \frac{\frac{1}{\frac{1}{R_l}+sC}}{\frac{1}{\frac{1}{R_l}+sC} + sL} = \frac{1}{1 + \frac{L}{R_l}s + s^2LC} = \frac{\omega_0^2}{s^2 + \frac{\omega_0}{Q_l} + \omega_0^2} \tag{E.13}$$

$$H_I(s) = \frac{\omega_0^2}{\left(s + \frac{\omega_0}{2Q_l}\right)^2 + \omega_0^2\left(1 - \frac{1}{4Q_l^2}\right)} = \frac{\omega_0}{\sqrt{1-\frac{1}{4Q_l^2}}}\frac{\omega_0\sqrt{1-\frac{1}{4Q_l^2}}}{\left(s + \frac{\omega_0}{2Q_l}\right)^2 + \omega_0^2\left(1 - \frac{1}{4Q_l^2}\right)} \tag{E.14}$$

$$h_i(t) = L^{-1}\{H_I(s)\} \tag{E.15}$$

$$h_i(t) = \frac{\omega_0}{\sqrt{1-\frac{1}{4Q_l^2}}}\mathrm{e}^{-\frac{\omega_0}{2Q_l}t}\sin\left(\omega_0\sqrt{1-\frac{1}{4Q_l^2}}t\right)\varepsilon(t) \tag{E.16}$$

$$k_{h_i}(t) = -j\frac{\omega_0}{\sqrt{1-\frac{1}{4Q_l^2}}}\mathrm{e}^{-\frac{\omega_0}{2Q_l}t}\varepsilon(t) \tag{E.17}$$

$$K_{H_I}(s) = \frac{\omega_0}{\sqrt{1-\frac{1}{4Q_l^2}}}\frac{-j}{s + \frac{\omega_0}{2Q_l}} \tag{E.18}$$

Appendix F

Analytic cavity energy stepresponse

$$\hat{i}_k(t) = \sqrt{\frac{2P_{tot}}{R_l}}\varepsilon(t) \tag{F.1}$$

$$g_{i_k}(t) = \hat{i}_k(t)e^{j\omega_{det}t} = \sqrt{\frac{2P_{tot}}{R_l}}\varepsilon(t) \tag{F.2}$$

$$G_{i_k}(s) = \sqrt{\frac{2P_{tot}}{R_l}}\frac{1}{s} \tag{F.3}$$

$$\frac{1}{2}G_{u_c}(s) = \frac{1}{2}G_{i_k}(s)\frac{1}{2}K_Z(s) \tag{F.4}$$

$$G_{u_c}(s) = \frac{1}{2}\sqrt{\frac{2P_{tot}}{R_l}}\frac{R_l\omega_0}{Q_l}\left\{\frac{1+j\frac{1}{2Q_l\sqrt{1-\frac{1}{4Q_l^2}}}}{s+\frac{\omega_0}{2Q_l}}\right\}\frac{1}{s} \tag{F.5}$$

$$G_{u_c}(s) = \frac{1}{2}\sqrt{\frac{2P_{tot}}{R_l}}\frac{R_l\omega_0}{Q_l}\left(1+j\frac{1}{2Q_l\sqrt{1-\frac{1}{4Q_l^2}}}\right)\frac{2Q_l}{\omega_0}\left\{\frac{1}{s}-\frac{1}{s+\frac{\omega_0}{2Q_l}}\right\} \tag{F.6}$$

$$g_{u_c}(t) = \frac{1}{2}\sqrt{\frac{2P_{tot}}{R_l}}\frac{R_l\omega_0}{Q_l}\left(1+j\frac{1}{2Q_l\sqrt{1-\frac{1}{4Q_l^2}}}\right)\frac{2Q_l}{\omega_0}\left\{1-e^{-\frac{\omega_0}{2Q_l}t}\right\} \tag{F.7}$$

$$\hat{u}_c(t) = |g_{u_c}(t)| = \sqrt{2P_{tot}R_l}\frac{1}{\sqrt{1-\frac{1}{4Q_l^2}}}\left\{1-e^{-\frac{\omega_0}{2Q_l}t}\right\} \approx \sqrt{2P_{tot}R_l}\left\{1-e^{-\frac{\omega_0}{2Q_l}t}\right\} \tag{F.8}$$

$$\langle w_C(t)\rangle_T = \frac{1}{4}C\left|\hat{u}_c(t)\right|^2 = \frac{1}{2}P_{tot}R_lC\left\{1-e^{-\frac{\omega_0}{2Q_l}t}\right\}^2 \tag{F.9}$$

$$\langle w_{st}(t)\rangle_T = P_{tot}R_lC\left\{1-e^{-\frac{\omega_0}{2Q_l}t}\right\}^2 = P_{tot}\frac{Q_l}{\omega_0}\left\{1-e^{-\frac{\omega_0}{2Q_l}t}\right\}^2 \tag{F.10}$$

Appendix G

The model derivation of the power modulator

G.1 linear laplace transformation

$$L_s \frac{dI_{mod}(t)}{dt} + I_{mod}(t)R_{eq} + \frac{1}{C_s}\int I_{mod}(t)dt = U_{steps}(t) \tag{G.1}$$

$$I_{mod}(t) = \frac{U_{mod}(t)}{R_{eq}} \tag{G.2}$$

$$\frac{L_s}{R_{eq}}\frac{d^2U_{mod}(t)}{dt^2} + \frac{dU_{mod}(t)}{dt} + \frac{1}{R_{eq}C_s}U_{mod}(t) = \frac{dU_{steps}(t)}{dt} \tag{G.3}$$

$$U_{mod}(s) = \mathcal{L}(U_{mod}(t)) \tag{G.4}$$

$$U_{mod}(s)\frac{L}{R_{eq}}\left(s^2 + \frac{R_{eq}}{L_s}s + \frac{1}{L_sC_s}\right) = sU_{steps}(s) \tag{G.5}$$

$$\frac{U_{mod}(s)}{U_{steps}(s)} = \frac{R_{eq}}{L_s}\frac{s}{s^2 + \frac{R_{eq}}{L_s}s + \frac{1}{L_sC_s}} \tag{G.6}$$

$$\omega_n = \frac{1}{\sqrt{L_sC_s}} \tag{G.7}$$

$$\zeta = \frac{R_{eq}}{2L_s\omega_n} = \frac{R_{eq}}{2}\sqrt{\frac{C_s}{L_s}} \tag{G.8}$$

$$\frac{U_{mod}(s)}{U_{steps}(s)} = \frac{2\zeta\omega_n s}{s^2 + 2\zeta\omega_n s + \omega_n^2} \tag{G.9}$$

$$U_{steps}(s) = \frac{U_{HV}}{s} \tag{G.10}$$

$$U_{mod}(s) = 2\zeta\omega_n U_{HV}\frac{1}{s^2 + 2\zeta\omega_n s + \omega_n^2} \tag{G.11}$$

$$U_{mod}(s) = \frac{2\zeta}{\sqrt{1-\zeta^2}} U_{HV} \frac{\omega_n \sqrt{1-\zeta^2}}{(s+\zeta\omega_n)^2 + \omega_n^2 (1-\zeta^2)} \tag{G.12}$$

$$U_{mod}(t) = \mathcal{L}^{-1} \left(U_{mod}(s) \right) \tag{G.13}$$

$$U_{mod}(t) = U_{HV} \frac{2\zeta}{\sqrt{1-\zeta^2}} e^{-\zeta\omega_n t} \sin\left(\omega_n \sqrt{1-\zeta^2} t\right) \tag{G.14}$$

G.2 Non-linear differential equations

$$-u_L(t) - u_C(t) - u_{mod}(t) = u_{steps}(t) \tag{G.15}$$

$$-L_s \frac{di_{mod}(t)}{dt} - u_C(t) - K^{-\frac{2}{3}} i_{mod}^{\frac{2}{3}}(t) = u_{steps}(t) \tag{G.16}$$

$$-L_s C_s \frac{d^2 u_C(t)}{dt^2} - u_C(t) - K^{-\frac{2}{3}} C_s^{\frac{2}{3}} \left(\frac{du_C(t)}{dt} \right)^{\frac{2}{3}} = u_{steps}(t) \tag{G.17}$$

$$i_{mod}(t) = C_s \frac{du_c(t)}{dt} \tag{G.18}$$

$$\frac{d^2 u_C(t)}{dt^2} = \frac{1}{L_s C_s} \left(u_{steps}(t) - u_C(t) - K^{-\frac{2}{3}} C_s^{\frac{2}{3}} \left(\frac{du_C(t)}{dt} \right)^{\frac{2}{3}} \right) \tag{G.19}$$

$$i_{mod}(t) = K u_{mod}^{\frac{3}{2}}(t) \tag{G.20}$$

$$p_{mod}(t) = K u_{mod}^{\frac{5}{2}}(t) \tag{G.21}$$

$$u_{mod}(t) = K^{-\frac{2}{3}} i_{mod}^{\frac{2}{3}}(t) \tag{G.22}$$

$$p_{mod}(t) = K^{-\frac{2}{3}} i_{mod}^{\frac{5}{3}}(t) \tag{G.23}$$

Bibliography

[Cou01] Leon W. Couch. *Digital and Analog Communication Systems/Leon W. Couch II.* Prentice Hall, New Jersey, sixth edition, 2001.

[K+01] F.B. Kiewiet et al. Femtosecond synchronization of a 3 GHz RF oscillator to a mode-locked Ti:sapphire laser. *Nuclear Instruments and Methods in Physics Research section A*, September 2001.

[P+91] Gun-Sik Park et al. Phase stability of gyroklystron amplifier. *IEEE transactions on plasma science*, 19(4):632–640, August 1991.

[Sla50] J.C. Slater. *Microwave Electronics.* Nostrand, Princeton, 1950.

[SP95] M.J. Smith and G. Phillips. *Power Klystrons Today.* Research studies press ltd., Taunton, Somerset, 1995.